https://doi.org/10.5194/gmd-2019-172
Preprint. Discussion started: 30 July 2019

Geoscientific Model Development Discussions

Beijing Climate Center Earth System Model version 1 (BCC-ESM1): Model Description and Evaluation

Tongwen Wu[1*], Fang Zhang[1], Jie Zhang[1], Weihua Jie[1], Yanwu Zhang[1], Fanghua Wu[1], Laurent Li[1,2], Xiaohong Liu[3], Xiao Lu[4], Lin Zhang[4], Jun Wang[5], Aixue Hu[6]

[1]Beijing Climate Center, China Meteorological Administration, Beijing, China
[2]Laboratoire de Météorologie Dynamique, IPSL, CNRS, Sorbonne Université, Ecole Normale Supérieure, Ecole Polytechnique, Paris, France
[3]University of Wyoming, Laramie, WY, USA
[4]Peking University, Beijing, China
[5] University of Iowa, Iowa City, IA 52242, USA
[6]National Center for Atmospheric Research, PO Box 3000, Boulder, Colorado 80307-3000, USA

Correspondence to: Tongwen Wu (twwu@cma.gov.cn)

https://doi.org/10.5194/gmd-2019-172
Preprint. Discussion started: 30 July 2019

Geoscientific Model Development Discussions

Abstract. BCC-ESM1 is the first version of a fully-coupled Earth System Model with interactive atmospheric chemistry and aerosols developed by Beijing Climate Center, China Meteorological Administration. Major aerosol species (including sulfate, organic carbon, black carbon, dust and sea salt) and greenhouse gases are interactively simulated with a whole panoply of processes controlling emission, transport, gas-phase chemical reactions, secondary aerosol formation, gravitational settling, dry deposition, and wet scavenging by clouds and precipitation. Effects of aerosols on radiation, cloud, and precipitation are fully treated. The performance of BCC-ESM1 in simulating aerosols and their optical properties is comprehensively evaluated as required by the Aerosol Chemistry Model Intercomparison Project (AerChemMIP), covering the preindustrial mean state and time evolution from 1850 to 2014. The simulated aerosols from BCC-ESM1 are quite coherent with CMIP5-recommended data and in-situ measurements from surface networks (such as IMPROVE in the U.S. and EMEP in Europe). A comparison of the aerosol optical depth (AOD) at 550 nm for all aerosols with the satellite AOD observations retrieved from MODIS and MISR and surface AOD observations from AERONET shows reasonable agreement between simulated and observed AOD. However, BCC-ESM1 seems to show weaker upward transport of aerosols from the surface to the middle and upper troposphere, likely reflecting the deficiency of representing deep convective transport of chemical species in BCC-ESM1. With an overall good agreement between BCC-ESM1 simulated and observed aerosol properties, it demonstrates a success of the implementation of interactive aerosol chemistry in BCC-ESM1.

https://doi.org/10.5194/gmd-2019-172
Preprint. Discussion started: 30 July 2019

Geoscientific Model Development Discussions

1. Introduction

Atmosphere is a thin gaseous layer around the Earth, consisting of nitrogen, oxygen and a large number of trace gases including important greenhouse gases (GHG) such as water vapor, tropospheric ozone (O_3), carbon dioxide (CO_2), methane (CH_4), nitrous oxide (N_2O), and chloro-fluoro-carbons (CFCs). Besides the gaseous components, atmosphere also contains various aerosols, which are important for cloud formation and radiative transfer. Atmospheric trace gases and aerosol particles are actually interactive components of the climate system. Their inclusion in climate models is a significant enhancement for most state-of-the-art climate models (Lamarque et al., 2013; Collins et al., 2017). Early attempts in coupling global climate dynamics with atmospheric chemistry can be traced back to late 1970s, when 3D transport of ozone and simple stratospheric chemistry were firstly incorporated into a GCM to simulate global ozone (O_3) production and transport (e.g., Cunnold et al. 1975; Schlesinger and Mintz 1979). Since mid-1980s, a large number of on-line global climate/chemistry models have been developed to address issues of the Antarctic stratospheric O3 depletion (e.g., Cariolle et al. 1990; Austin et al. 1992; Solomon, 1999), tropospheric O3 and sulfur cycle (e.g., Feichter et al. 1996; Barth et al. 2000), tropospheric aerosol and its interactions with cloud (e.g., Chuang et al. 1997; Lohmann et al. 2000; Ghan and Easter, 2006; Jacobson 2012). Aerosols and chemically reactive gases in the atmosphere exert important influences on global and regional air quality and climate (Collins et al., 2017).

Since 2013, the Beijing Climate Center (BCC), China Meteorological Administration, has continuously developed and updated its global fully-coupled climate model, the Beijing Climate Center Climate System Model (BCC-CSM) (Wu et al., 2013). BCC-CSM version 1.1 was one of the comprehensive carbon-climate models participating to the phase five of the Coupled Model Intercomparison Project (CMIP5, Taylor et al. 2012). When forced by prescribed historical emissions of CO_2 from combustion of fossil fuels and land use change, BCC-CSM1.1 successfully reproduced the trends of observed atmospheric CO_2 concentration and global surface air temperature from 1850 to 2005 (Wu et al., 2013). During recent years, BCC-CSM1.1 has been used in numerous investigations on soil organic carbon changes (e.g. Todd-Brown et al., 2014), ocean biogeochemistry changes (e.g. Mora et al., 2013), and

https://doi.org/10.5194/gmd-2019-172
Preprint. Discussion started: 30 July 2019

carbon-climate feedbacks (e.g. Arora et al., 2013; Hoffman et al., 2014). BCC-CSM includes main climate-carbon cycle processes (Wu et al., 2013) and the global mean atmospheric CO_2 concentration is calculated from a prognostic equation of CO_2 budget taking into account global anthropogenic CO_2 emissions and interactive land-atmosphere and ocean-atmosphere CO_2 exchanges.

In recent years, BCC has put much efforts in developing a global climate-chemistry-aerosol fully-coupled Earth System Model (BCC-ESM) on the basis of BCC-CSM. The objective is to interactively simulate global aerosols (e.g. sulfate, black carbon, etc.) and main greenhouse gases (e.g. O_3, CH_4, NO_2 and CO_2) in the atmosphere and to investigate feedbacks between climate and atmospheric chemistry. BCC-ESM1 is at the point to be publicly released, and it is actively used in BCC for several CMIP6-endorsed research initiatives (Eyring et al. 2016), including the Aerosol Chemistry Model Intercomparison Project (AerChemMIP, Collins et al., 2017) and the Coupled Climate–Carbon Cycle Model Intercomparison Project (C4MIP, Jones et al. 2016).

The purpose of this paper is to evaluate the performance of BCC-ESM1 to simulate aerosols and their optical properties in the 20th century. The description of BCC-ESM1 is presented in Section 2. The experimental protocol is shown in Section 3. Section 4 presents evaluations of aerosol simulations with comparisons to CMIP5-recommended data and data from both global surface networks and satellite observations. The regional and global characteristics compared to observations and estimates from other studies are analyzed. Simulations of aerosol optical properties in the 20th century are also analyzed in Section 4. Conclusions and discussions are summarized in Section 5. Information about code and data availability is shown in Section 6.

2. Model description

BCC-ESM1 is a fully-coupled global climate-chemistry-aerosol model. The atmospheric component is BCC Atmospheric General Circulation Model version 3 (Wu et al., 2019) with interactive atmospheric chemistry (hereafter BCC-AGCM3-Chem). The oceanic component is the Modular Ocean Model version 4 with 40 levels (hereafter MOM4-L40). The land component is BCC Atmosphere and Vegetation Interaction Model version 2.0 (BCC-AVIM2.0) with terrestrial carbon cycle. The sea ice component is Sea Ice Simulator

https://doi.org/10.5194/gmd-2019-172
Preprint. Discussion started: 30 July 2019

Geoscientific Model Development Discussions

(SIS). Different components of BCC-ESM1 interact with each other through fluxes of momentum, energy, water, carbon and other tracers at their interfaces. The coupling between the atmosphere and the ocean is done every hour. BCC-AGCM3-Chem is able to simulate global atmospheric composition and aerosols with anthropogenic emissions as forcing. It is developed on the basis of the recent version 3 of the Beijing Climate Center atmospheric general circulation model (hereafter BCC-AGCM3, Wu et al., 2019). The horizontal resolution of BCC-AGCM3-Chem is T42 (approximately 2.8125° x2.8125° transformed spectral grid). The model has 26 levels in a hybrid sigma/pressure vertical coordinate system with the top level at 2.914 hPa. The land component BCC-AVIM2.0 is described in details in Li et al. (2019). It includes biophysical, physiological, and soil carbon-nitrogen dynamical processes, and the terrestrial carbon cycle operates through a series of biochemical and physiological processes on photosynthesis and respiration of vegetation. Biogenic emissions from vegetation are computed online in BCC-AVIM2.0 following the algorithm of the Model of Emissions of Gases and Aerosols from Nature version 2.1 (MEGAN2.1, Guenther et al., 2012). Details of oceanic component MOM4-L40 and sea-ice component SIS that are used in BCC-ESM1 may be found in Wu et al. (2013) and Wu et al. (2019). MOM4-L40 used a tripolar grid of horizontal resolution with 1 °longitude by 1/3 °latitude between 30 °S and 30 °N ranged to 1 ° latitude at 60 °S and 60 °N and 40 z-levels in the vertical. Carbon exchange between the atmosphere and the ocean are calculated online in MOM4-L40 using a biogeochemistry module that is based on the protocols from the Ocean Carbon Cycle Model Intercomparison Project–Phase 2 (OCMIP2, http://www.ipsl.jussieu.fr/OCMIP/phase2/). SIS has the same horizontal resolution as MOM4-L40 and three layers in the vertical, including one layer of snow cover and two layers of equally sized sea ice.

The BCC-AGCM3-Chem combines 66 gas-phase chemical species and 13 bulk aerosol compounds as listed in Table 1. Apart from 2 gas-phase species of dimethyl sulfide (DMS) and SO_2, the other 63 gas-phase species are the same as those in the "standard version" of MOZART2 (Model for Ozone and Related chemical Tracers, version 2), a global chemical transport model for the troposphere developed by the National Center for Atmospheric Research (NCAR) driven by meteorological fields from either climate models or assimilations of meteorological observations (Horowitz et al., 2003). Advection of all tracers in

https://doi.org/10.5194/gmd-2019-172
Preprint. Discussion started: 30 July 2019

Geoscientific Model Development Discussions

BCC-AGCM3-Chem is performed through a semi-Lagrangian scheme (Williamson and Rasch, 1989), and vertical diffusion within the boundary layer follows the parameterization of Holtslag and Boville (1993). The gas-phase chemistry of the 63 MOZART2 gas-phase species as listed in Table 1 is treated in the same way as in the "standard version" of MOZART2 (Horowitz et al., 2003). There are 33 photolytic reactions and 135 chemical reactions involving 30 dry deposited chemical species and 25 soluble gas-phase species. Their dry depositions are calculated following the resistance-in-series approach originally described in Wesely (1989). Dry deposition velocities for the 15 trace gases including O3, CO, CH4, CH2O, CH3OOH, H2O2, NO2, HNO3, PAN, CH3COCH3, CH3COOOH, CH3CHO, CH3COCHO, NO, and HNO4 are directly interpolated from MOZART2 climatological monthly mean deposition velocities, and those for the other 15 species are determined using a weighted-combination of deposition velocities of ozone, CO, or CH3CHO. Wet removals by in-cloud scavenging for 25 soluble gas-phase species in the "standard version" of MOZART2 use the parameterization of Giorgi and Chameides (1985) based on their temperature dependent effective Henry's law constants. In-cloud scavenging is proportional to the amount of cloud condensate converted to precipitation, and the loss rate depends on the amount of cloud water, the rate of precipitation formation, and the rate of tracer uptake by the liquid phase water. Other highly soluble species such as HNO3, H2O2, ONIT, ISOPOOH, MACROOH, XOOH, and Pb-210 are also removed by below-cloud washout as calculated using the formulation of Brasseur et al. (1998). Below-cloud scavenging is proportional to the precipitation flux in each layer and the loss rate depends on the precipitation rate. Vertical transport of gas tracers and aerosols due to deep convection is not yet included in the present version of BCC-AGCM3-Chem.

In the following sub-sections, we will describe the treatments in BCC-ESM1 for 2 gas-phase species of DMS and SO_2, 13 prognostic aerosol species including sulfate (SO_4^{2-}), 2 types of organic carbon (hydrophobic OC1, hydrophilic OC2), 2 types of black carbon (hydrophobic BC1, hydrophilic BC2), 4 categories of soil dust (DST01, DST02, DST03, DST04), and 4 categories of sea salt (SSLT01, SSLT02, SSLT03, SSLT04). Concentrations of all aerosols in BCC-ESM1 are mainly determined by advective transport, emission, dry deposition, gravitational settling, and wet scavenging by clouds and precipitation, except for

https://doi.org/10.5194/gmd-2019-172
Preprint. Discussion started: 30 July 2019

Geoscientific Model Development Discussions

SO_4^{2-} which gas-phase chemical reactions and aqueous phase conversion from SO_2 are also considered. The present version of aerosols belongs to a bulk aerosol type of model, and the nucleation and coagulation of aerosols are still ignored in the present version of BCC-AGCM3-Chem of BCC-ESM1.

2.1 SO_2, DMS, and Sulfate

SO_2 is a main sulfuric acid precursor to form aerosol sulfate SO_4^{2-}. Conversions of SO_2 to SO_4^{2-} occur by gas phase reactions (Table 2) and by aqueous phase reactions in cloud droplets. The dry deposition velocity of SO_2 follows the resistance-in-series approach of Wesely (1989) using the formula, $W_{SO2} = 1/(r_a + r_c)$, in which r_a and r_c are the aerodynamic resistance and the surface canopy layer resistance, respectively. The loss rate of SO_2 due to wet deposition is computed following the scheme in the global Community Atmosphere Model (CAM) version 4, the atmospheric component of the Community Earth System Model (Lamarque, et al., 2012).

The sources of SO_2 mainly come from fuel combustion, industrial activities, and volcanoes. SO_2 can also be formed from the oxidation of DMS as listed in Table 2. The main source of DMS is from oceanic emissions via biogenic processes. It is prescribed using the MOZART2 data package originated from the International Global Atmospheric Chemistry/Global Emissions Inventory Activity (IGAC/GEIA, Benkovitz et al., 1996).

SO_4^{2-} is one of the prognostic aerosols in BCC-AGCM3-Chem. It is produced primarily by the gas-phase oxidation of SO_2 (in Table 2) and by aqueous phase oxidation of SO_2 in cloud droplets. The gas phase reactions, rate constants, and gas-aqueous equilibrium constants are given by Tie et al. (2001). The heterogeneous reactions of SO_4^{2-} occur on all aerosol surfaces. Their treatment follows a Bulk Aerosol Model (BAM) used in CAM4 (Neale et al., 2010). The heterogeneous reactions depend strongly on pH values in clouds which are calculated from the concentrations of SO_2, HNO_3, H_2O_2, NH_3, O_3, HO_2, and SO_4^{2-}. Only NH_3 is not a prognostic tracer in BCC-AGCM3-Chem and it is estimated using the assumption of an NH_3 to SO_4^{2-} molar ratio of 2.0. SO_4^{2-} is assumed to be all in aqueous phase, although Wang et al. (2008a) showed that ~34% of sulfate particles are in solid phase globally due to the hysteresis effect of ammonium sulfate phase transition. However, in terms of radiative forcing, consideration of solid sulfate formation process lowers the sulfate forcing by ~8% as

https://doi.org/10.5194/gmd-2019-172
Preprint. Discussion started: 30 July 2019

Geoscientific Model Development Discussions

compared to consideration of all sulfate particles in aqueous phase (Wang et al., 2008b). Future model development may consider the life cycle of NH_3. The sulfate in- and below-cloud scavenging follows Neu and Prather (2011). Washout of SO_4^{2-} is set to 20% of the washout rate of HNO_3 following Tie et al. (2005) and Horowitz (2006). Its dry deposition velocity of SO_4^{2-} is also calculated by the resistance-in-series approach.

2.2 Aerosols of organic carbon and black carbon

BCC-AGCM3-Chem treats two types of organic carbon (OC), i.e. water-insoluble tracer OC1 and water-soluble tracer OC2, and two types of black carbon (BC), i.e. water-insoluble tracer BC1 and water-soluble tracer BC2. As shown in Table 2, hydrophobic BC1 and OC1 can be converted to hydrophilic BC2 and OC2 with a constant rate of 7.1×10^{-6} s^{-1} (Cooke and Wilson, 1996). The 4 tracers of organic carbon and black carbon are mainly from emissions of anthropogenic activities including both fossil fuel and biomass burning, and are from the CMIP6 data package (https://esgf-node.llnl.gov/search/input4mips/). Beside anthropogenic emissions, hydrophilic organic carbon OC2 can also come directly from natural biogenic volatile organic compound (VOC) emissions. They are calculated online in the land component model BCC-AVIM2 and assumed to equal to 10% of monoterpenes emission following the algorithm of Guenther et al. (1999).

Dry deposition velocities for all the 4 OC and BC tracers are set to 0.001m.s^{-1}. OC2 and BC2 are soluble aerosols, and their sinks are primarily governed by wet deposition. Their in- and below-cloud scavenging follows the scheme of Neu and Prather (2011) and the transfer of soluble gases into liquid condensate is calculated with Henry's Law assuming equilibrium between the gas and liquid phases.

2.3 Sea salt aerosols

As shown in Table 3, sea salt aerosols in the model are classified into four size bins (0.2–1.0, 1.0–3.0, 3.0–10, and 10–20 μm) in diamater. They originate from oceans and are calculated online by BCC-ESM1. The upward flux $F_{sea-salt}$ of sea salt productions for four bins is proportional to the 3.41 power of the wind speed u_{10m} at 10 m height near the sea surface (Mahowald et al., 2006) and is expressed as

$$F_{sea-salt} = S \cdot (u_{10m})^{3.41}, \quad (1)$$

where S is a scaling factor prescribed for each bin of sea salt aerosol.

https://doi.org/10.5194/gmd-2019-172
Preprint. Discussion started: 30 July 2019


Geoscientific Model Development Discussions

Dry deposition of sea salts depends on the turbulent deposition velocity in the lowest atmospheric layer using aerodynamic resistance and the friction velocity, and the settling velocity through the whole atmospheric column for each bin of sea salts. The turbulent deposition velocity and settling velocity depend on particle diameter and density (listed in Table 3). In addition, the fact that the size of sea salts changes with humidity is also considered. The wet deposition of sea salts follows the scheme for soluble aerosols used in CAM4, and depends on prescribed solubility and size-independent scavenging coefficients.

2.4 Dust aerosols

Dust aerosols behave in a similar way as sea salts. Their variations involve three major processes: emission, advective transport, and wet/dry depositions. The dust emission is based on a saltation-sandblasting process, and depends on wind friction velocity, soil moisture, and vegetation/snow cover (Zender et al., 2003). The vertical flux of dust emission is corrected by a surface erodible factor at each model grid cell which has been downloaded from NCAR website (https://ncar.ucar.edu/). Soil erodibility is prescribed by a physically-based geomorphic index that is proportional to the runoff area upstream of each source region (Albani et al., 2014). Like sea salts, dry deposition includes gravitational and turbulent deposition processes, while wet deposition results from both convective and large scale precipitation and is dependent on prescribed size-independent scavenging coefficients.

2.5 Effects of aerosols on radiation, cloud, and precipitation

The mass mixing ratios of bulk aerosols are prognostic variables in BCC-ESM1 and directly affect the shortwave radiative transfer in the atmosphere with their treatments following the NCAR Community Atmosphere Model (CAM3, Collins et al., 2004). Indirect effects of aerosols are taken into account in the present version of BCC-AGCM3-Chem (Wu et al., 2019). Aerosol particles act as cloud condensation nuclei and exert influence on cloud properties and the hydrological cycle, and ultimately impact precipitation. The liquid cloud droplet number concentration is an important factor in determining the effective radius of cloud droplets for radiative calculation and in calculating the precipitation efficiency. As described for BCC-AGCM3 in Wu et al. (2019), it is parameterized as an empirical function of cloud water content and bulk aerosol mass concentration (Boucher and Lohmann, 1995; Quaas et al., 2006).

https://doi.org/10.5194/gmd-2019-172
Preprint. Discussion started: 30 July 2019

3. Experiment design for the 20th century climate simulation

To assess the ability of our model to simulate aerosols (mean and variability), we have followed the historical simulation designed by AeroChemMIP. The AeroChemMIP historical case is a simulation with emissions evolving from 1850 to 2014 and with specified GHG concentrations of CH_4, N_2O, and CO_2 following the protocols defined by CMIP6. Other historical forcing data include: (1) monthly zonally-mean CFC11 and CFC12 concentrations, (2) yearly global gridded land-use forcing data sets, and (3) solar forcing. All these datasets were downloaded from https://esgf-node.llnl.gov/search/input4mips/. The principal GHGs for radiation calculation in BCC-AGCM-Chem1 include H_2O, O_3, CH_4, N_2O, CO_2, CFC11 and CFC12. Only one GHG, O_3, is a prognostic variable at each model step and interacts with radiations.

3.1 Surface emissions

Surface emissions of chemical species from different sources are summarized in Table 4. They include anthropogenic emissions from fossil fuel burning and other industrial activities, biomass burning (including vegetation fires, fuel wood and agricultural burning), biogenic emissions from vegetation and soils, and oceanic emissions. Most historical emissions from anthropogenic source (surface, airplane plus ships) and biomass burning in the period of 1850 to 2014 are CMIP6-recommended data (Hoesly et al., 2017; available at https://esgf-node.llnl.gov/search/input4mips). Anthropogenic or biomass burning sources of some tracers not included in CMIP6 data are from the standard package of MOZART-2 or the IPCC ACCMIP emission inventory (http://accent.aero.jussieu.fr/ACCMIP.php) covering the period from 1850 to 2010 in 10-year time intervals. CMIP6-recommended emissions of black carbon and organic carbon aerosols assume 80% in hydrophobic form and 20% in hydrophilic form following Chin et al. (2002).

Seven tracers in Table 1 belong to biogenic volatile organic carbons (VOCs), i.e. ISOP, ACET (CH_3COCH_3), C_2H_4, C_2H_6, C_3H_{10}, Terpenes ($C_{10}H_{16}$), and OC_2. As shown in Table 4, those VOCs emissions are directly online calculated in BCC-ESM1 following the modeling framework of the Model of Emissions of Gases and Aerosols from Nature version 2.1 (MEGAN2.1, Guenther et al., 2012) using simple mechanistic algorithms to account for major known processes controlling biogenic emissions. The MEGAN emissions depend on current

https://doi.org/10.5194/gmd-2019-172
Preprint. Discussion started: 30 July 2019


Geoscientific Model Development Discussions

and past surface air temperature and solar flux, and their calculation requires global maps of plant functional type (PFT) and leaf area index (LAI) which is a prognostic variable from the land model BCC-AVIM2.

3.2 Volcano eruption, lightning and aircraft emissions

Emissions of stratospheric SO_2 from volcanic eruption from 1850 to 2014 are prescribed using the CMIP6-recommended data, although recent studies based on satellite observation of SO_2 in 2006-2012 have revealed that this emission data may have a factor of 2-4 high bias in average (Ge et al., 2016). Aircraft emissions are provided for NO_2, CO, CH_4, and SO_2 (Table 1). The emissions of NO from lightning are online calculated in BCC-AGCM3-Chem following the parameterization in MOZART2. The lightning frequency depends strongly on the convective cloud top height, and the ratio of cloud-to-cloud versus cloud-to-ground lightning depends on the cold cloud thickness from 0°C to the cloud top (Price and Rind, 1992).

3.3 Upper boundary of the atmosphere

As no stratospheric chemistry is included in the present version of BCC-AGCM3-Chem, it is necessary to ensure a proper distribution of chemically-active stratospheric species including O_3, CH_4, N_2O, NO, NO_2, HNO_3, CO, and N_2O_5. Concentrations of those tracers at the top two layers of the model are set to prescribed climatological values, and with a 10-day time scale down to the tropopause. Climatological values of NO, NO_2, HNO_3, CO and N_2O_5 at the top two model levels use MOZART2 data package and are based on Study of Transport and Chemical Reactions in the Stratosphere (STARS, Brasseur et al., 1997). Concentrations of ozone, CH_4, and N_2O at the top two model levels are the zonally and monthly values derived from the CMIP6 data package.

3.4 The preindustrial model states

The preindustrial state of BCC-ESM1 is obtained from a piControl simulation of over 600 years in which all forcings including emissions data are fixed at 1850 AD conditions. The initial state of the piControl simulation itself is obtained through individual spin-up runs of each component of BCC-ESM1 in order for the piControl simulation to run stably and fast to reach its equilibrium. Figures 1(a-b) show the time series of surface air temperature and the net energy budget at top of the model (TOM) from the piControl simulation for the last 450

https://doi.org/10.5194/gmd-2019-172
Preprint. Discussion started: 30 July 2019

years. It shows that the surface climate in BCC-ESM1 nearly reaches its equilibrium after 600 years piControl simulation. The whole system in BCC-CSM1 fluctuates around +0.7 W m^{-2} net energy flux at TOM without obvious trend in 600 years (Fig. 1b), and the global mean surface air temperature shows only a small warming (Fig. 1a). During the last 450 years, there are (±0.2 ℃ amplitude) oscillations of centennial scale for the whole globe, which are certainly caused by internal variation of the system.

Figures 2a-2c show the time series of global annual total masses of SO_2, DMS, and OH in the troposphere (integrated from the surface to 100 hPa) in the last 450 years of the piControl simulation. Without any anthropogenic source, the SO_2 amount in the troposphere nearly varies around 0.0868±0.002 Tg in the 450 years of the piControl simulation. Tropospheric DMS varies around the value of 0.116±0.002 Tg. Tropospheric OH, as an important gas species oxidizing SO_2 to form SO_4^{2-} (Table 2), keeps at a stable level in the atmosphere. SO_4^{2-} also remains at a stable level of 0.556±0.004 Tg in the atmosphere in the whole period of the piControl simulation . Without any anthropogenic source, the amounts of BC and OC in the troposphere vary around 0.0395±0.005 Tg and 0.275±0.005 Tg, respectively. Dust and sea salt aerosols are at the level of 22±1 Tg and 11.7±1 Tg, respectively. All those data are close to the CMIP5 recommended concentrations in year 1850 (0.604 Tg SO_4^{2-}, 0.046 Tg BC, 0.30 Tg OC, 22.18 Tg dust, and 11.73 Tg sea salts).

Figure 3 shows the global spatial distributions of annual mean sulfate, organic carbon, black carbon, dust, and sea salt aerosols in the whole atmospheric column averaged for the last 100 years of the piControl simulation of BCC-ESM. We can compare them with CMIP5 recommended concentrations in year 1850, considered as the reference state in the pre-industrial stage. Without any industrial and fossil fuel anthropogenic emissions of SO_2, the SO_4^{2-} is mainly distributed over the tropical Pacific and Atlantic Oceans. There are several centers of high values of black carbon and organic carbon in East and South Asia, Europe, Southeast America, and in the tropical rain forests in Africa and South America. They mainly result from biomass burning including vegetation fires, fuel wood and agricultural burning. Dust aerosols are mainly distributed in North Africa, Central Asia, North China, and Australia, where arid and semi-arid areas locate. Dust emitted from Sahara Desert can be transported to the tropical Atlantic by easterly wind. The sea salt aerosols are mainly distributed over the

https://doi.org/10.5194/gmd-2019-172
Preprint. Discussion started: 30 July 2019


Geoscientific Model Development Discussions

mid-latitude Southern Oceans, the tropical southern Indian Ocean, and the tropical northern Pacific Ocean, where wind speeds near the sea surface are strong. As shown in Fig. 3, all the spatial distribution patterns of CMIP5-derived sulfate, black carbon, organic carbon, dust, and sea salt aerosols are well simulated in BCC-ESM1, and there are high spatial correlation coefficients, 0.76 for sulfate, 0.77 for black carbon, 0.77 for organic carbon, 0.94 for dust, and 0.94 for sea salts, between CMIP5 data and BCC-ESM1 simulations.

4. Evaluation of aerosols simulation in the 20th century

4.1 Global aerosols trends

Figure 4(a)-(c) show the time series of global total emissions of SO_2, OC, BC to the atmosphere from natural and anthropogenic sources. Emissions of SO_2 are largely related to industrial production. From 1850 to 1915, SO_2 emissions increased year by year as the Industrial Revolution intensified and expanded. But from 1915 to 1945, the increase trend of SO_2 emissions evidently became slower as broke out the First and the Second World Wars. After that period, with growing industrial productions, SO_2 emissions increased again and reached a maximum around the end of 1970s. During the 1980s and 2000s, with a substantial decrease of SO_2 emissions in Europe and the United States, the global SO_2 emissions has been decreasing since the 1980s despite the rapid increase of SO_2 emissions in South and East Asia as well as in developing countries in the Southern Hemisphere in recent years (Liu et al., 2009). The OC and BC emissions substantially increased since 1950s just after the Second World War. The global total OC emission in 2010 was nearly twice as much as that in pre-industrial (year 1850) and increased by 18 Tg yr^{-1}. Anthropogenic black carbon emissions increased from 1 Tg yr^{-1} in 1850 to nearly 8 Tg yr^{-1} in 2010.

Anthropogenic SO_2, OC and BC emissions strongly affect the variations of atmospheric concentrations DMS, SO_2, sulfate, OC, and BC. As shown in Figure 5b-5f, the annual total aerosol masses of SO_4^{2-}, OC, and BC in the whole atmosphere column as simulated by the BCC-ESM 20th century historical simulation are generally consistent with the CMIP5-recommended aerosols masses. Due to increasing SO_2 emissions from 1850 to present day (Fig. 4), the global SO_2 burden in the atmosphere increased from 100 Tg in 1850s to 200 Tg in 1980s (Fig. 5a), and has a high interannual correlation coefficient of 0.996 with the anthropogenic emissions (Fig. 4a). DMS in the atmosphere is oxidized by OH and NO_3 to

https://doi.org/10.5194/gmd-2019-172
Preprint. Discussion started: 30 July 2019


Geoscientific Model Development Discussions

form SO_2 (Table 2). Its natural emissions from oceans from 1850 to 2010 in the model are the climatological monthly means from NCAR data package. As shown in Fig 5a, the global amount of DMS in the whole atmosphere was about 0.12 Tg during 1850-1900 and decreased to 0.055 Tg in 2010. This decrease trend possibly results from the prescribed emissions have not year-to-year variations and the loss of DMS oxidation to produce SO_2 gradually exceeds the source (Table 5) as the rate of DMS oxidation reaction (Table 2) gets large along with global warming in the 20th century. Largely driven by SO_2 anthropogenic emissions, the sulfate burden shows three different stages from 1850 to present. In the first period from 1850s to 1900s, the sulfate burden had a weak linear increase. It increased significantly in the second stage from 1910's to 1940's, and then exploded since 1950's, until the middle 1970s and earlier 1980s. The sulfate burden then remained nearly stable and even showed slightly decreases as seen from the CMIP5 data. The trends of global BC and OC burdens are similar to that of sulfate, but they showed continuous increases from 1950 to present.

The dust and sea salt aerosols in the atmosphere are largely determined by the atmospheric circulations and states of the land and ocean surface. We can see that the global dust burden in the atmosphere showed a large interannual variability and was slightly enhanced from 1950 to 2000, which could be partly caused by global warming and increasing soil dryness resulting in more surface dust to be released in the atmosphere.

4.2 Global aerosols budgets

We further evaluate global aerosols budgets by comparing a 10-year average of BCC-ESM results from 1990 to 2000 with various observational data for sulfate, BC, OC, sea salt, and dust. Their annual total emissions, average atmospheric mass loading, and mean lifetimes are listed in Tables 5 and 6. It is worth emphasizing that the global mean total source and sink for each type of aerosols in BCC-ESM1 are almost balanced.

The global DMS emission from the ocean is 27.4 Tg S yr^{-1} in BCC-ESM. It is higher than the value reported in Liu et al (2005), largely due to stronger wind speed near the sea surface. This high emission in BCC-ESM is nearly balanced by the gas-phase oxidation of DMS to form SO_2. The DMS burden is 0.06 Tg S with a lifetime of 0.78 days, which is within the range of other models reported in the literature. As shown in Table 5, the total SO_2 production averaged for the period of 1991 to 2000 is 76.93 Tg S yr^{-1}. A rate of 13.2 Tg S yr^{-1}

https://doi.org/10.5194/gmd-2019-172
Preprint. Discussion started: 30 July 2019


Geoscientific Model Development Discussions

(about 17%) is produced from the DMS oxidation, only 0.1 Tg S yr^{-1} from air traffic, and the rest (63.63 Tg S yr^{-1}, near 82.7%) from anthropogenic activities. Here the emissions of SO_2 from volcanic eruption are not included. The amount of SO_2 produced from the DMS oxidation is in the range of other works (10.0 to 24.7 Tg S yr^{-1}) reported in Liu et al (2005). All the SO_2 production is balanced by SO_2 losses by dry and wet deposition, and by gas- and aqueous-phase oxidation. Half of its loss (38.74 Tg S yr^{-1}) occurs via its aqueous-phase oxidation to form sulfate. Other losses through dry and wet depositions and gas-phase oxidation to form SO_4^{2-} are also important (Table 2). All the sinks are in the range from the literature (Liu et al., 2005). The global burden of SO_2 in the atmosphere is 0.24 Tg S with a lifetime of 1.12 days, consistent with values in literature (Liu et al., 2005).

Sulfate aerosol is mainly produced from aqueous-phase SO_2 oxidation (38.73 Tg S yr^{-1}) and partly from gaseous phase oxidation of SO_2 (10.32 Tg S yr^{-1}), and is largely lost by wet scavenging (49.06 Tg S yr-1). The total SO_4^{2-} production in BCC-ESM is at the lower range of values in other models reported in Textor et al. (2006). Its global burden is 0.63 Tg S and the lifetime is 4.69 days, which are within the range of 0.57 to 0.66 Tg S and 3.72 to 5.4 days in the literatures (Textor et al., 2006; Liu et al., 2012; Liu et al., 2009; the value derived from CMIP5 data).

Sources of BC and OC are mainly from anthropogenic emissions. Based on the CMIP6 data, there are, on average, 7.22 Tg yr^{-1} BC and 45.2 Tg yr^{-1} OC from fossil and bio-fuel emissions during the period of 1991 to 2000. Most of them are scavenged through convective and large-scale rainfall processes. The rest returns to the surface by dry deposition. The simulated BC and OC lifetimes are 6.6 and 5.0 days, respectively. The simulated global BC and OC burdens are 0.13 and 0.62 Tg, respectively (Table 6), all close to values of 0.114 Tg BC and 0.69 Tg OC derived from the CMIP5 data.

The annual total dust emission in BCC-ESM1 is 2592 Tg yr^{-1}, higher than AeroCom multi-model mean (1840 Tg yr^{-1}, Textor et al., 2006), but comparable to other studies (Chin et al., 2002; Liu et al., 2012; Emmons et al., 2010). The average dust loading is 22.93 Tg, lower than the value of 35.9 Tg in Ginoux et al. (2001) but slightly higher than the CMIP5 data. The average lifetime for dust particles is 3.23 days that is shorter than the AeroCom mean (4.14 days). The simulated sea salt emission is 4667.2 Tg yr^{-1}, slightly lower than the

https://doi.org/10.5194/gmd-2019-172
Preprint. Discussion started: 30 July 2019


Geoscientific Model Development Discussions

simulated value in Liu et al. (2012), and substantially lower than the AeroCom mean (16600 Tg yr−1, Textor et al., 2006).

4.3 Global aerosol distributions at present day

Figures 6-10 show December-January-February (DJF) and June-July-August (JJA) mean column mass concentrations of sulfate ($SO4^{2-}$), OC, BC, Dust, and Sea Salt aerosols averaged for the period of 1991-2000, respectively. Here, BCC-ESM1 simulated results are compared with the CMIP5-recommended data for the same period. Unlike the pre-industrial level of sulfate shown in Fig. 2, sulfate concentrations at present day (Fig. 6) are strongly influenced by anthropogenic emissions, and have maximum concentrations in the industrial regions (e.g., East Asia, Europe, and North America). Their seasonal variations are distinct and are characterized by high concentrations in boreal summer and low levels in winter. These spatial distributions simulated by BCC-ESM1 are well consistent with the CMIP5 data, with spatial correlation coefficients in DJF and JJA reaching 0.92 and 0.83, respectively.

Unlike sulfate whose maximum concentrations are mainly distributed between 60 ℃N and the equator, peaking concentrations of BC and OC as shown in Figs. 7 and 8 are located near the tropics in the biomass burning regions (e.g., the maritime continent, Central Africa, South America), and their seasonal variations from DJF to JJA are evidently weaker than those of sulfate except in South America. In boreal summer, there are centers of high values in the industrial regions in the Northern Hemisphere mid-latitudes (i.e., East Asia, South Asia, Europe, and North America). These main features of spatial and seasonal variations in CMIP5 data are well captured by BCC-ESM1, and the BCC-ESM1 vs. CMIP5 spatial correlation coefficients are 0.90 (OC in DJF), 0.91 (BC in DJF), 0.91 (OC in JJA) and 0.92 (BC in JJA).

As show in Figure 9, dust concentrations in the atmosphere show largest values over strong source regions such as Northern Africa, Southwest and Central Asia, and Australia, and over their outflow regions such as the Atlantic and the western Pacific. In DJF, the CMIP5 data shows centers of high concentrations over East Asia and Central North America, but both centers are missing in BCC-ESM1. We think, however, that these two high-value centers in the CMIP5 data may not be true, since frozen soils in these areas in winter lead to unfavorable conditions for soil erosion by wind. The spatial correlation coefficients between CMIP5 and BCC-ESM1 remain high: 0.95 in JJA and 0.88 in DJF.

https://doi.org/10.5194/gmd-2019-172
Preprint. Discussion started: 30 July 2019


Geoscientific Model Development Discussions

As shown in Figure 10, high sea salt concentrations are generally over the storm track regions over the oceans, e.g., middle-latitudes in the Northern Oceans in DJF and the Southern Ocean in JJA where wind speeds and thus sea salt emissions are higher. In addition, there is a belt of high sea salt concentrations in the subtropics of both hemispheres where precipitation scavenging is weak. Their spatial distributions in BCC-ESM1 are consistent with the CMIP5 data with correlation coefficients of 0.92 in JJA and 0.90 in DJF.

Figure 11 shows vertical profiles of zonally-averaged annual mean concentrations of sulfate, organic carbon, black carbon, dust, and sea salt aerosols in the period of 1991-2000. Both BCC-ESM1 and CMIP5 results show that strong sulfur, OC, and BC emissions in the industrial regions of the Northern Hemisphere mid-latitudes can rise upward and be transported towards the North Pole in the middle to upper troposphere. Most of OC, BC, and dust aerosols are confined below 500 hPa, while sulfate can be transported to higher altitudes. Sea salt aerosols are mostly confined below 700 hPa, as the particles are large and favorable for wet removal and gravitational settling towards the surface. It can be seen that BCC-EMS1 tends to simulate less upward transport of aerosols than the CMIP5 data, likely reflecting the omission of deep convection transport of tracers in BCC-ESM1.

The CMIP5 data used here are mainly from model simulations. We need to further evaluate the BCC-ESM1 model results with ground observations. Annual mean SO_4^{2-}, BC and OC aerosol concentration observations from the Interagency Monitoring of Protected Visual Environments (IMPROVE) sites over 1990-2005 in the United States (http://vista.cira.colostate.edu/IMPROVE/) and from the European Monitoring and Evaluation Programme (EMEP) (http://www.emep.int) sites over 1995-2005 are used. As shown in Figure 12a and 12b, the BCC-ESM simulated sulfate concentrations are in general comparable to the EMEP observations in Europe, but are systematically about 1 μg m^{-3} higher than the U.S. IMPROVE observations. As for BC, there are large model biases at both European and U.S. sites (Figs. 12c and 12d), especially BCC-ESM overestimates BC concentrations at the IMPROVE sites. The simulated OC concentrations are slightly overestimated for IMPROVE sites but systematically underestimated for EMEP sites. These comparisons are overall fairly reasonable considering the uncertainties in emissions and the coarse model resolution.

https://doi.org/10.5194/gmd-2019-172
Preprint. Discussion started: 30 July 2019

4.4 Aerosol Optical Properties

Aerosol optical depth is an indicator of the reduction in incoming solar radiation (at a particular wavelength) due to scattering and absorption of sunlight by aerosols. In this study, we calculate the aerosol optical depth (AOD) at 550 nm for all aerosols including sulfate, BC, Organic Carbon, sea salt and dust as the product of aerosol dry mass concentrations and their specific extinction coefficients. The total AOD is calculated by summing the AOD in each model layer for each aerosol species using the assumption that they are externally mixed.

The aerosol optical depth (AOD) observations retrieved from MODIS and MISR are used to evaluate the 1997-2003 averaged AOD in BCC-ESM. Figure 13 shows averages of MISR and MODIS AOD with corresponding averages from BCC-ESM. The BCC-ESM1 simulated AOD generally captures the spatial distribution of MISR and MODIS retrievals. The model overestimates AOD over East China. It also systematically underestimates the MODIS observations in the Southern Hemisphere, but is closer to MISR observations.

Figure 14 compares the monthly AOD values at 550 nm from BCC-ESM with 1998–2005 averaged monthly observations from AERONET (http://aeronet.gsfc.nasa.gov) at sites in Europe, North America, East Asia, and South Asia. Model simulated monthly AOD generally agrees with observations within a factor of 2 for most sites. BCC-ESM slightly overestimates the AOD in European (43.4-55.4 ℃N and 7.6-27.6 ℃E) and North American (43.4-55.4 ℃N and 7.6-27.6 ℃E) sites. In those regions, BCC-ESM also slightly overestimates MODIS and MISR AOD observations (Fig. 13).

5. Summary and discussions

This paper presented a comprehensive evaluation of aerosols simulated in version 1 of the Beijing Climate Center Earth System Model (BCC-ESM1) with the implementation of the interactive atmospheric chemistry and aerosol based on the newly developed BCC-CSM2. Global aerosols (including sulfate, organic carbon, black carbon, dust and sea salt) and major greenhouse gases (e.g., O_3, CH_4, N_2O) in the atmosphere are interactively simulated when anthropogenic emissions are provided to the model. Concentrations of all aerosols in BCC-ESM1 are determined by the processes of advective transport, emission, gas-phase chemical reactions, dry deposition, gravitational settling, and wet scavenging by clouds and precipitation. The nucleation and coagulation of aerosols are ignored in the present version of

https://doi.org/10.5194/gmd-2019-172
Preprint. Discussion started: 30 July 2019


Geoscientific Model Development Discussions

525 BCC-ESM1. Effects of aerosols on radiation, cloud, and precipitation are fully included.

526 We evaluated the performance of BCC-ESM1 in simulating aerosols and their optical
527 properties in the 20th century following the requirement of the Aerosol Chemistry Model
528 Intercomparison Project (AerChemMIP). The AeroChemMIP historical simulation uses
529 anthropogenic emissions evolving from 1850 to 2014 and prescribes GHG concentrations
530 (e.g., CH_4, N_2O, CO_2, CFC11 and CFC12) using CMIP6-recommended data. Both direct and
531 indirect effects of aerosols are considered in BCC-ESM1. Initial conditions of the
532 AeroChemMIP historical simulation are obtained from a 600-year piControl simulation in the
533 absence of anthropogenic emissions, which well captures the pre-industrial concentrations of
534 sulfate (SO_4^{2-}), organic carbon (OC), black carbon (BC), dust, and sea salt aerosols and are
535 consistent with the CMIP5 recommended concentrations for the year 1850.

536 With the CMIP6 anthropogenic emissions of SO_2, OC, BC from 1850 to 2014 and their
537 natural emissions implemented in BCC-ESM1, the model simulated SO_4^{2-}, BC, and OC
538 aerosols in the atmosphere are highly correlated with the CMIP5-recommended data. The
539 long-term trends of CMIP5 aerosols from 1850 to 2000 are also well simulated by
540 BCC-ESM1. Global budgets of aerosols were evaluated through comparisons of BCC-ESM1
541 results for 1990-2000 with various observational data at present day for sulfate, BC, OC, sea
542 salt, and dust. Their annual total emissions, global atmospheric mass loading, and mean
543 lifetimes are all within the range of values reported in relevant literatures.

544 Evaluations of the spatial and vertical distributions of BCC-ESM1 simulated present-day
545 sulfate (SO_4^{2-}), OC, BC, Dust, and Sea Salt aerosol concentrations against the CMIP5 datasets
546 and in-situ measurements of surface networks (IMPROVE in the U.S. and EMEP in Europe)
547 indicate good agreement among them. The BCC-ESM1 simulates weaker upward transport of
548 aerosols from the surface to the middle and upper troposphere (with reference to
549 CMIP5-recommended data), likely reflecting a lack of deep convection transport of chemical
550 species in the present version of BCC-ESM1. The aerosol optical depth (AOD) at 550 nm for
551 all aerosols including sulfate, BC, OC, sea salt, and dust aerosols was further compared with
552 the satellite AOD observations retrieved from MODIS and MISR and surface AOD
553 observations from AERONET. The BCC-ESM1 model results are overall in good agreement
554 with these observations within a factor of 2. All these comparisons demonstrate the success of

https://doi.org/10.5194/gmd-2019-172
Preprint. Discussion started: 30 July 2019

the implementation of interactive aerosol chemistry in BCC-ESM1.

This work has only evaluated the ability of BCC-ESM1 to simulate aerosols. The variations of aerosols especially for sulfate are related to other gaseous tracers such as OH and NO_3 (Table 2), which are determined by the MOZART2 gaseous chemical scheme as implemented in BCC-ESM1 and require further evaluation. How about the GHGs simulations in the AeroChemMIP historical run? Can the global warming be reproduced? These questions concerning feedbacks of prognostic aerosols on climate change especially global warming also need to be explored in the future.

6. Code and data availability

Source codes of BCC-ESM1 model are freely available upon request addressed to Tongwen Wu (twwu@cma.gov.cn). Model output of BCC CMIP6 AerChemMIP simulations described in this paper is distributed through the Earth System Grid Federation (ESGF) and freely accessible through the ESGF data portals after registration. Details about ESGF are presented on the CMIP Panel website at http://www.wcrp-climate.org/index.php/wgcm-cmip/about-cmip.

Author contributions

Tongwen Wu led the BCC-ESM1 development. All other co-authors have contributions to it. Fang Zhang and Jie Zhang designed the experiments and carried them out. Tongwen Wu, Laurent Li, Lin Zhang, Xiaohong Liu, Aixue Hu, and Jun Wang wrote the final document with contributions from all other authors.

Acknowledgements

This work was supported by The National Key Research and Development Program of China (2016YFA0602100). All the figures are created by the NCAR Command Language (Version 6.6.2) [Software].

References

Albani, S., Mahowald, N. M., Perry, A. T., Scanza, R. A., Zender, C. S., Heavens, N. G., Maggi, V., Kok, J. F., and Otto-Bliesner, B. L.: Improved dust representation in the

https://doi.org/10.5194/gmd-2019-172
Preprint. Discussion started: 30 July 2019

585 Community Atmosphere Model, J. Adv. Model. Earth Syst., 6, 541–570,
586 doi:10.1002/2013MS000279, 2014.
587 Arora, V., Boer, G., Friedlingstein, P., Eby, M., Jones, C., Christian, J., Bonan, G., Bopp, L.,
588 Brovkin, V., Cadule, P., Hajima, T., Ilyina, T., Lindsay, K., Tjiputra, J., and Wu, T.:
589 Carbon-concentration and carbon-climate feedbacks in CMIP5 Earth system models. J.
590 Climate, 26, 5289–5314, 2013.
591 Austin, J., Butchart, N., and Shine, K. P.: Possibility of an Arctic ozone hole in a
592 doubled-CO2 climate, Nature, 360, 221–225, 1992
593 Barth, M.C., Rasch, P.J., Kiehl, J.T., Benkowitz, C.M., and Schwartz, S.E.: Sulfur chemistry
594 in the National Center for Atmospheric Research Community Climate Model:
595 Description, evaluation, features, and sensitivity to aqueous chemistry. J. Geophys. Res.,
596 105, D1, 1387-1415, 2000.
597 Benkovitz, C.M., Scholtz, M.T., Pacyna, J., Tarrasón, L., Dignon, J., Voldner, E.V., Spiro,
598 P.A., Logan, J.A., and Graedel, T.E.: Global Gridded Inventories of Anthropogenic
599 Emissions of Sulfur and Nitrogen, J. Geophys. Res., 101 (D22), 29239-29253, 1996.
600 Boucher, O., Lohmann, U.: The sulphate-CCN-cloud albedo effect – a sensitivity study with
601 two general circulation models, Tellus 47B, 281–300, 1995.
602 Brasseur, G. P., Hauglustaine, D. A., Walters, S., Rasch, P. J., Mu ller, J.-F., Granier, C., and
603 Tie, X. X.: MOZART, a global chemical transport model for ozone and related chemical
604 tracers: 1. Model description, J. Geophys. Res., 103, 28,265– 28,289, 1998.
605 Brasseur, G. P., Tie, X. X., Rasch, P. J., and Lefèvre, F.: A three-dimensional simulation of
606 the Antarctic ozone hole: Impact of anthropogenic chlorine on the lower stratosphere and
607 upper troposphere, J. Geophys. Res., 102, 8909–8930, 1997.
608 Cariolle, D., Lasserre-Bigorry, A., and Royer, J.-F.: A general circulation model simulation of
609 the springtime Antarctic ozone decrease and its impact on midlatitudes, J. Geophys. Res.,
610 95, 1883–1898, 1990.
611 Chuang, C. C., Penner, J. E., Taylor, K. E., Grossman, A. S., and Walton, J. J.: An assessment
612 of the radiative effects of anthropogenic sulfate, J. Geophys. Res., 102, 3761–3778,
613 1997.
614 Collins, W. J., Lamarque, J.–F., Schulz, M., Boucher, O., Eyring, V., Hegglin, M. I.,
615 Maycock, A., Myhre, G., Prather, M., Shindell, D., Smith, S. J.: AerChemMIP:
616 quantifying the effects of chemistry and aerosols in CMIP6, Geosci. Model Dev., 10,

https://doi.org/10.5194/gmd-2019-172
Preprint. Discussion started: 30 July 2019

585–607, 2017.

Collins, W. D., Rasch, P. J., Boville, B. A., Hack, J. J., McCaa, J. R., Williamson, D. L,. Kiehl, J. T., Briegleb, B. P., Bitz, C., Lin, S.-J., Zhang, M., and Dai, Y.: Description of the NCAR Community Atmosphere Model (CAM3). Nat. Cent. for Atmos. Res., Boulder, Colo., 2004.

Cooke, W.F., Wilson, J.J.N.: A global black carbon aerosol model. J. Geophys. Res. Atmos. 101, 19395–19409, 1996.

Cunnold D., Alyea, F., Phillips, N., Prinn, R.: A three-dimensional dynamical-chemical model of atmospheric ozone, J. Atmos. Sci., 32, 170-194, 1975.

Eyring, V., Bony, S., Meehl, G. A., Senior, C. A., Stevens, B., Stouffer, R. J., and Taylor, K. E.: Overview of the Coupled Model Intercomparison Project Phase 6 (CMIP6) experimental design and organization, Geosci. Model Dev., 9, 1937–1958, doi:10.5194/gmd-9-1937-2016, 2016.

Feichter J., Kjellstrom, E., Rodhe, H., Dentener, F., Lelieveldi, J., Roelofs, G.-J.: Simulation of the tropospheric sulfur cycle in a global climate model, 30: 1693-1707, 1996.

Ge, C., Wang, J., Carn, S., Yang, K., Ginoux, P., Krotkov, N.: Satellite-based global volcanic SO2 emissions and sulfate direct radiative forcing during 2005–2012, J. Geophys. Res. Atmos., 121, 3446–3464, doi:10.1002/2015JD023134, 2016.

Ghan S. J. and Easter, R. C.: Impact of cloud-borne aerosol representation on aerosol direct and indirect effects, Atmos. Chem. Phys., 6, 4163–4174, 2006.

Giorgi, F., and Chameides, W. L.: The rainout parameterization in a photochemical model, J. Geophys. Res., 90, 7872–7880, 1985.

Guenther, A. B., Jiang, X., Heald, C. L., et al.: The Model of Emissions of Gases and Aerosols from Nature Version 2.1 (MEGAN2.1): An Extended and Updated Framework for Modeling Biogenic Emissions. Geoscientific Model Development 5(6): 1471–1492, 2012.

Guenther, A., Baugh, B. Brasseur, G., Greenberg, J., Harley, P., Klinger, L,. Serca, D., and Vierling, L.: Isoprene emission estimates and uncertainties for the Central African EXPRESSO study domain, J. Geophys. Res., 104(D23), 30,625–30,639, 1999.

Guenther, A. B., et al.: A global model of natural volatile organic compound emissions, J. Geophys. Res., 100, 8873–8892, 1995.

Horowitz, L.W., Walters, S., Mauzerall, D. L., Emmons, L. K., Rasch, P. J., Granier, C., Tie,

https://doi.org/10.5194/gmd-2019-172
Preprint. Discussion started: 30 July 2019

X., Lamarque, J.-F., Schultz, M. G., Tyndall, G. S., Orlando, J. J., Brasseur, G. P.: A global simulation of tropospheric ozone and related tracers: Description and evaluation of MOZART, version 2, J. Geophys. Res., 108(D24), 4784, doi:10.1029/2002JD002853, 2003.

Horowitz, L. W.: Past, present, and future concentrations of tropospheric ozone and aerosols: Methodology, ozone evaluation, and sensitivity to aerosol wet removal, J. Geophys. Res., 111, D22211, doi:10.1029/2005JD006937, 2006.

Hoesly, R. M., Smith, S. ., Feng, L., Klimont, Z., Janssens-Maenhout, G., Pitkanen, T., Seibert, J. J., Vu, L., Andres, R. J., Bolt, R. M., Bond, T. C., Dawidowski, L., Kholod, N., Kurokawa, J., Li, M., Liu, L., Lu, Z., Moura, M. C. P., O'Rourke, R. R., and Zhang Q.: Historical (1750–2014) anthropogenic emissions of reactive gases and aerosols from the Community Emission Data System (CEDS), Geosci. Model Dev., 11, 369-408, 2018

Hoffman, F. M., Randerson, J. T., Arora, V. K., Bao, Q., Cadule, P., Ji, D., Jones, C. D., Kawamiya, M., Khatiwala, S., Lindsay, K., Obata, A., Shevliakova, E., Six, K. D., Tjiputra, J. F., Volodin, E. M., and Wu, T.: Causes and implications of persistent atmospheric carbon dioxide biases in Earth System Models, J. Geophys. Res. Biogeosci., 119, 141–162, doi:10.1002/2013JG002381, 2014.

Holtslag, A. A. M., and Boville, B. A.: Local versus nonlocal boundary-layer diffusion in a global climate model, J. Climate, 6, 1825–1842, 1993.

Jacobson, M.Z.: Investigating cloud absorption effects: global absorption properties of black carbon, tar balls, and soil dust in clouds and aerosols. J. Geophys. Res. 117, D06205, 2012.

Jones C.D., Arora, V., Friedlingstein, P., Bopp, L., Brovkin, V., Dunne, J., Graven, H., Hoffman, F., Ilyina, T., John, J. G., Jung, M., Kawamiya, M., Koven, C., Pongratz, J., Raddatz, T., Randerson, J. T., and Zaehle, S.: C4MIP – The Coupled Climate–Carbon Cycle Model Intercomparison Project: experimental protocol for CMIP6, Geosci. Model Dev., 9, 2853–2880, doi:10.5194/gmd-9-2853-2016, 2016.

Lamarque, J.-F., Shindell, D. T., Josse, B., Young, P. J., Cionni, I., Eyring, V., Bergmann, D., Cameron-Smith, P., Collins,W. J., Doherty, R., Dalsoren, S., Faluvegi, G., Folberth, G., Ghan, S. J., Horowitz, L. W., Lee, Y. H., MacKenzie, I. A., Nagashima, T., Naik, V., Plummer, D., Righi, M., Rumbold, S. T., Schulz, M., Skeie, R. B., Stevenson, D. S., Strode, S., Sudo, K., Szopa, S.,Voulgarakis, A., and Zeng, G.: The Atmospheric

https://doi.org/10.5194/gmd-2019-172
Preprint. Discussion started: 30 July 2019

Chemistry and Climate Model Intercomparison Project (ACCMIP): overview and description of models, simulations and climate diagnostics, Geosci. Model Dev., 6, 179–206, doi:10.5194/gmd-6-179-2013, 2013.

Lamarque, J.-F., Emmons, L. K., Hess, P. G., Kinnison, D. E., Tilmes, S., Vitt, F., Heald, C. L., Holland, E. A., Lauritzen, P. H., Neu, J., Orlando, J. J., Rasch, P. J., and Tyndall, G. K.: CAM-chem: description and evaluation of interactive atmospheric chemistry in the Community Earth System Model, Geosci. Model Dev., 5, 369–411, 2012

Lohmann, U., Feichter, J., Penner, J. E., and Leaitch, W. R.: Indirect effect of sulfate and carbonaceous aerosols: A mechanistic treatment. J. Geophys. Res, 105, 12193–12206, 2000

Li, W., Zhang, Y., Shi, X., Zhou, W., Huang, A., Mu, M., Qiu, B., JI, J.: Development of the Land Surface Model BCC_AVIM2.0 and Its Preliminary Performance in LS3MIP/CMIP6, J. Meteor. Res., (in press), 2019.

Liu, X. H., Penner, J. E., and Herzog, M.: Global modeling of aerosol dynamics: Model description, evaluation, and interactions between sulfate and nonsulfate aerosols, J. Geophys. Res.-Atmos., 110, D18206, doi:10.1029/2004jd005674, 2005.

Liu, J., Mauzerall, D.L., Horowitz, L.W., Ginoux, P., Fiore, A.M.: Evaluation intercontinental transport of fine aerosols: (1) methodology, global aerosol distribution and optical depth. Atmos Environ 43:4327–4338, 2009.

Madronich, S.: Photodissociation in the atmosphere 1. Actinic flux and the effect of ground reflections and clouds, J. Geophys. Res., 92, 9740–9752, 1987.

Mahowald, N., Lamarque, J.-F., Tie, X., and Wolff, E.: Sea salt aerosol response to climate change: last glacial maximum, preindustrial and doubled carbon dioxide climates, J. Geophys. Res., 111, D05303, doi:10.1029/2005JD006459, 2006.

Mora, C., Wei, C.-L., Rollo, A., Amaro, T., Baco, A.R., Billett, D., Bopp, L., Chen, Q., Collier, M., Danovaro, R., Gooday, A.J., Grupe, B.M., Halloran, P.R., Ingels, J., Jones, D.O.B., Levin, L.A., Nakano, H., Norling, K., Ramirez-Llodra, E., Rex, M., Ruh, H.A., Smith, C.R., Sweetman, A.K., Thurber, A.R., Tjiputra, J. F., Usseglio, P., Watling, L., Wu, T., Yasuhara, M.: Biotic and human vulnerability to projected ocean biogeochemistry change over the 21st century, PLoS Biol 11(10): e1001682. doi:10.1371/journal.pbio.1001682, 2013.

NCAR Command Language (Version 6.6.2) [Software], Boulder, Colorado:

https://doi.org/10.5194/gmd-2019-172
Preprint. Discussion started: 30 July 2019

713 UCAR/NCAR/CISL/TDD. http://dx.doi.org/10.5065/D6WD3XH5, 2019.
714 Neale, R. B., et al.: Description of the NCAR Community Atmosphere Model (CAM 4.0),
715 NCAR Tech. Note, TN-485, pp. 212, Natl. Cent. for Atmos. Res., Boulder, Colo., 2010
716 Neale, R. and co-authors: Description of the NCAR Community Atmosphere Model
717 (CAM5.0). NCAR/TN-486+STR, NCAR Technical Note, 2012.
718 Neu, J. L. and Prather, M. J.: Toward a more physical representation of precipitation
719 scavenging in global chemistry models: cloud overlap and ice physics and their impact
720 on tropospheric ozone, Atmos. Chem. Phys. Discuss., 11, 24413–24466,
721 doi:10.5194/acpd-11-24413-2011, 2011.
722 Price, C., and Rind, D.: A simple lightning parameterization for calculating global lightning
723 distributions, J. Geophys. Res., 97, 9919-9933, 1992.
724 Quaas, J., Boucher, O., and Lohmann, U.: Constraining the total aerosol indirect effect in
725 the LMDZ and ECHAM4 GCMs using MODIS satellite data. Atmos Chem Phys 6,947–
726 955, 2006.
727 Sander, S., Friedl, R. R., Ravishankara, A. R., et al.: Chemical Kinetics and Photochemical
728 Data for Use in Atmospheric Studies, Evaluation Number 14, JPL Publication 02-25,
729 NASA, Jet Propulsion Laboratory, California Institute of Technology, Pasadena, CA,
730 2003.
731 Schlesinger, M. E., Mintz, Y.: Numerical simulation of ozone production, transport and
732 distribution with a global atmospheric general circulation model, J.Atmos.Sci., 36:
733 1325-1361, 1979.
734 Solomon, S.: Stratospheric ozone depletion: A review of concepts and history, Reviews of
735 Geophysics, 37, 275–316, 1999.
736 Taylor, K.E., Stouffer, R. J., Meehl, G. A.: An overview of CMIP5 and the experiment design,
737 Bull. Am. Meteorol. Soc. 93, 485-498, 2012.
738 Tie, X., Brasseur, G., Emmons, L., Horowitz, L., and Kinnison, D.: Effects of aerosols on
739 tropospheric oxidants: A global model study, J. Geophys. Res., 106, 2931– 2964, 2001.
740 Tie, X., Madronich, S., Walters, S., Edwards, D., Ginoux, P., Mahowald, N., Zhang, R., Luo,
741 C., and Brasseur, G.: Assessment of the global impact of aerosols on tropospheric
742 oxidants, J. Geophys. Res., 110, D03204, doi:10.1029/2004JD005359, 2005.
743 Todd-Brown, K.E.O., Randerson, J.T., Hopkins, F., Arora, V., Hajima, T., Jones, C.,
744 Shevliakova, E., Tjiputra, J., Volodin, E., Wu, T., Zhang, Q., Allison, S.D.: Changes in

https://doi.org/10.5194/gmd-2019-172
Preprint. Discussion started: 30 July 2019

soil organic carbon storage predicted by Earth system models during the 21st century, Biogeosciences, 11, 2341-2356, 2014.

Wang, J., Hoffmann, A. A., Park, R., Jacob, D. J., and Martin, S. T.: Global distribution of solid and aqueous sulfate aerosols: effect of the hysteresis of particle phase transitions, J. Geophys. Res., 113, D11206, Doi:11210.11029/12007JD009367, 2008a.

Wang, J., Jacob, D. J., and Martin, S. T.: Sensitivity of sulfate direct climate forcing to the hysteresis of particle phase transitions, J. Geophys. Res., 113, D11207, doi:11210.11029/12007JD009368, 2008b.

Wesely, M. L.: Parameterization of surface resistance to gaseous dry deposition in regional-scale numerical models, Atmos. Environ., 23, 1293–1304, 1989.

Williamson, D. L., and Rasch, P. J.: Two-dimensional semi-Lagrangian transport with shapepreserving interpolation, Mon. Wea. Rev., 117, 102–129, 1989.

Wu, T., Song, L., Li, W., Wang, Z., Zhang, H., Xin, X., Zhang, Y., Zhang, L., Li, J., Wu, F., Liu, Y., Zhang, F., Shi, X., Chu, M., Zhang, J., Fang, Y., Wang, F., Lu, Y., Liu, X., Wei, M., Liu, Q., Zhou, W., Dong, M., Zhao, Q., Ji, J., Li, L., Zhou, M.: An overview of BCC climate system model development and application for climate change studies. J. Meteor. Res., 28(1), 34-56, 2014.

Wu, T., Li, W., Ji, J., Xin, X., Li, L., Wang, Z, Zhang, Y., Li, J., Zhang, F., Wei, M., Shi, X., Wu, F., Zhang, L., Chu, M., Jie, W., Liu, Y., Wang, F., Liu, X., Li, Q., Dong, M., Liang, X., Gao, Y., Zhang, J.: Global carbon budgets simulated by the Beijing climate center climate system model for the last century. J Geophys Res Atmos, 118, 4326-4347. doi: 10.1002/jgrd.50320, 2013.

Wu, T., Yu, R., Zhang, F., Wang, Z., Dong, M., Wang, L., Jin, X., Chen, D., Li, L.: The Beijing Climate Center atmospheric general circulation model: description and its performance for the present-day climate, Climate Dynamics, 34, 123-147, DOI 10.1007/s00382-008-0487-2, 2010.

Zender, C., Bian, H., and Newman, D.: Mineral Dust Entrainment and Deposition (DEAD) model: Description and 1990s dust climatology, J. Geophys. Res., 108(D14), 4416, doi: 10.1029/2002JD002775, 2003.

https://doi.org/10.5194/gmd-2019-172
Preprint. Discussion started: 30 July 2019

Geoscientific Model Development Discussions

775 Table 1. Chemical species considered in BCC-AGCM3-Chem. Species marked with star (*)
776 denote those added in BCC-ESM1 apart from the 63 species used in MOZART2.
777

Species		Dry deposition	Wet deposition	Surface emission	Airplane emission	Volcanic emission
Gas tracers	O_3	√				
	N_2O			√		
	N					
	NO	√		√		
	NO_2	√			√	
	NO_3					
	HNO_3	√	√			
	HO_2NO_2	√	√			
	N_2O_5					
	CH_4	√		√	√	
	CH_3O_2					
	CH_3OOH	√	√			
	CH_2O	√	√	√		
	CO	√		√	√	
	OH					
	HO_2					
	H_2O_2	√	√			
	C_3H_6			√		
	ISOP			√		
	PO_2					
	CH_3CHO	√	√			
	POOH	√	√			
	CH_3CO_3					
	CH_3COOOH	√	√			
	PAN	√				
	ONIT	√	√			
	C_2H_6			√		
	C_2H_4			√		
	C_4H_{10}			√		
	MPAN	√				
	$ISOPO_2$					
	MVK		√			
	MACR		√			
	$MACRO_2$					
	MACROOH	√	√			
	MCO_3					
	$C_2H_5O_2$					
	C_2H_5OOH	√	√			
	$C_{10}H_{16}$			√		

778

779

https://doi.org/10.5194/gmd-2019-172
Preprint. Discussion started: 30 July 2019

Geoscientific Model Development Discussions

780 Table 1. Continued.

Species name		Dry deposition	Wet deposition	Surface emission	Airplane emission	Volcanic emission
Gas tracers	C_3H_8					
	$C_3H_7O_2$					
	C_3H_7OOH	√	√			
	CH_3COCH_3	√		√		
	ROOH		√			
	CH_3OH	√	√	√		
	C_2H_5OH	√	√			
	GLYALD	√	√			
	HYAC	√	√			
	EO2					
	EO					
	HYDRALD	√	√			
	RO_2					
	CH3COCHO	√	√			
	Rn-222					
	Pb-210	√	√			
	$ISOPNO_3$		√			
	ONITR	√	√			
	XO_2					
	XOOH	√	√			
	ISOPOOH	√	√			
	H_2	√		√		
	Stratospheri	√				
	Inert O_3	√				
	SO_2*	√	√	√	√	√
	DMS*			√		
Aerosols	SO_4^{2-}*	√	√			
	OC1*	√	√	√		
	OC2*	√	√	√		
	BC1*	√	√	√		
	BC2*	√	√	√		
	SSLT01*	√	√			
	SSLT02*	√	√			
	SSLT03*	√	√			
	SSLT04*	√	√			
	DST01*	√	√			
	DST02*	√	√			
	DST03*	√	√			
	DST04*	√	√			

781
782

https://doi.org/10.5194/gmd-2019-172
Preprint. Discussion started: 30 July 2019

Geoscientific Model Development Discussions

Table 2. Gas-phase chemical reactions for bulk aerosols precursors. The reaction rates (s^{-1}) refer to Tie et al. (2001) and Sander et al. (2003), Chin et al. (1996), and Cooke and Wilson (1996). Temperature (T) is expressed in K, air density (M) in molecule cm^{-3}, ki and ko in cm^3 $molecule^{-1}$ s^{-1}.

Chemical reactions	Rate
SO2 + OH → SO4	ko/(1.+ko*M/ki)*f**(1./(1.+log10(ko*M/ki)), in which ko=3.0E-31*(300/T)**3.3; ki=1.E-12; f =0.6
DMS + OH → SO2	9.60E-12*exp(-234./T)
DMS + OH → .5*SO2 + .5*HO2	1.7E−42*exp(7810/T)*M*0.21/(1+5.5E−31*exp(7460/T)* M* 0.21)
DMS + NO3 → SO2 + HNO3	1.90E-13*exp(520/T)
BC1 → BC2	7.10E-06
OC1 → OC2	7.10E-06

https://doi.org/10.5194/gmd-2019-172
Preprint. Discussion started: 30 July 2019

Geoscientific Model Development Discussions

790

791 Table 3. Size and density parameters of bulk aerosols.

792

Aerosols	Species Name	Mean radius (μm) / bin size (μm)	Geometric standard deviation (μm)	Density (g cm^{-3})
SO4	Sulfate	0.05	2.03	1.77
BC1	hydrophobic black carbon	0.02	2.00	1.0
BC2	hydrophilic black carbon	0.02	2.00	1.0
OC1	hydrophobic organic carbon	0.03	2.24	1.8
OC2	hydrophilic organic carbon	0.03	2.24	1.8
DST01	Dust	0.55/ bin: 0.1-1.0	2.00	2.5
DST02	Dust	1.75 / bin: 1.0-2.5	2.00	2.5
DST03	Dust	3.75 / bin: 2.5-5.0	2.00	2.5
DST04	Dust	7.50 / bin: 5.0-10.	2.00	2.5
SSLT01	Sea salt	0.52 / bin: 0.2-1.0	2.00	2.2
SSLT02	Sea salt	2.38 / bin: 1.0-3.0	2.00	2.2
SSLT03	Sea salt	4.86 / bin: 3.0-10.	2.00	2.2
SSLT04	Sea salt	15.14 / bin: 10.-20.	2.00	2.2

793

https://doi.org/10.5194/gmd-2019-172
Preprint. Discussion started: 30 July 2019

Geoscientific Model Development Discussions

Table 4. Source of surface emission data. MOZART2 data denote the standard tropospheric chemistry package for MOZART contains surface emissions from the EDGAR 2.0 data base (Olivier et al., 1996). ACCMIP data are downloaded from the IPCC ACCMIP emission inventory (http://accent.aero.jussieu.fr/ACCMIP.php) and they vary from 1850 to 2000, in 10-year steps (Lamarque et al., 2010). CMIP6 data are from https://esgf-node.llnl.gov/search/input4mips/. Anthropogenic emission includes Industrial and fossil fuel use, agriculture, ships, and etc. Biomass burning includes vegetation fires incl. fuel wood and agricultural burning.

Species	Anthropogenic emission	Biomass burning	Biogenic emissions from vegetation	Biogenic emissions from soil	Oceanic emissions
C2H4	CMIP6	CMIP6	On-line computation		MOZART2
C2H5OH	CMIP6	CMIP6			
C2H6	CMIP6	CMIP6	ACCMIP		MOZART2
C3H6	CMIP6	CMIP6	On-line computation		MOZART2
C3H8	CMIP6	CMIP6	ACCMIP		MOZART2
C4H10	CMIP6	ACCMIP	MOZART2		MOZART2
CH2O	CMIP6	CMIP6			
CH3CHO	ACCMIP	CMIP6			
CH3COCHO		CMIP6			
CH3OH	ACCMIP	CMIP6	ACCMIP		
CH4	CMIP6	CMIP6	MOZART2	MOZART2	MOZART2
CO	CMIP6	CMIP6	ACCMIP	MOZART2	ACCMIP
H2	ACCMIP	CMIP6		MOZART2	
N2O	MOZART2	CMIP6		MOZART2	MOZART2
NH3	CMIP6	CMIP6			
NO	CMIP6	CMIP6		ACCMIP	
SO_2	CMIP6	CMIP6			
DMS					ACCMIP
OC1	CMIP6	CMIP6			
OC2	CMIP6	CMIP6	On-line computation		
BC1	CMIP6	CMIP6			
BC2	CMIP6	CMIP6			
ACET	ACCMIP	ACCMIP	On-line computation		MOZART2
ISOP		ACCMIP	On-line computation		
Terpenes		CMIP6	On-line computation		

https://doi.org/10.5194/gmd-2019-172
Preprint. Discussion started: 30 July 2019

Geoscientific Model Development Discussions

Table 5. Global budgets for DMS, SO2, and sulfate in the period of 1991 to 2000. Units are sources and sinks, Tg S yr^{-1}; burden, Tg S; lifetime, days.

		BCC-ESM (1991-2000 mean)	Other studies and CMIP5 data
DMS	Sources	27.4	
	Emission	27.4	10.7-23.7[a]
	Sinks	28.0	
	Gas-phase oxidation	28.0	10.7-23.7[a]
	Burden	0.06	0.02-0.15[a]
	Lifetime	0.78	0.5-3.0[a]
SO_2	Sources	76.93	
	Emission at surface	63.63	
	Emission from airplane	0.10	
	DMS oxidation	13.20	10.0-24.7[a]
	Sinks	76.96	
	Dry deposition	18.53	16.0-55.0[a]
	Wet deposition	9.36	0.0-19.9[a]
	Gas-phase oxidation	10.33	6.1-16.8[a]
	Aqueous-phase oxidation	38.74	24.5-57.8[a]
	Burden	0.24	0.20-0.61[a]
	Lifetime	1.12	0.6-2.6[a]
SO_4^{2-}	Sources	49.05	59.67±13.13[b]
	Emission	0.00	
	SO_2 aqueous-phase oxidation	38.73	
	SO2 gas-phase oxidation	10.32	
	Sinks	49.06	
	Dry deposition	2.20	4.96-5.51[d]
	Wet deposition	46.86	39.34-40.20[d]
	Burden	0.63	0.66±0.16[b], 0.57[c], 0.61[e]
	Lifetime	4.69	4.12±0.74[b], 3.72-3.77[d] 5.4[e]

Notes: References denote a, Liu et al. (2005); b, Textor et al., 2006; c. derived from CMIP5 prescribed aerosol masses averaged from 1991 to 2000; d. Liu et al. (2012); e. Liu et al. (2009).

https://doi.org/10.5194/gmd-2019-172
Preprint. Discussion started: 30 July 2019

Geoscientific Model Development Discussions

Table 6. Same as Table 5, but for global budgets for black carbon, organic carbon, dust, and sea salts. Units are sources and sinks, Tg yr^{-1}; burden, Tg; lifetime, days.

		BCC-ESM (1991-2000 mean)	Other studies and CMIP5 data
BC	Sources	7.22	
	Emission	7.22	
	Sinks	7.24	7.75[d]
	Dry deposition	0.90	
	Wet deposition	6.34	
	Burden	0.13	0.114[c], 0.24±0.1[a]
	Lifetime	6.60	7.12±2.35[d], 5.8[e]
OC	Sources	45.20	
	Fossil and bio-fuel emission	45.20	
	Sinks	45.22	50.1[d]
	Dry deposition	3.41	
	Wet deposition	41.81	
	Burden	0.62	0.69[c], 1.70±0.45[a]
	Lifetime	5.00	4.56−4.90[d], 5.3[e], 6.54±1.76[a]
Dust	Sources	2592.0	1840[b], 2943.5−3121.9[d]
	Sinks	2592.0	
	Dry deposition	1630.8	
	Wet deposition	961.2	
	Burden	22.93	20.41[c], 22.424.7[d], 35.9[f]
	Lifetime	3.23	2.61−3.07[d], 4.14±1.78[a]
Sea Salt	Sources	4667.2	4965.5-5004.1[d]
	Sinks	4667.4	
	Dry deposition	2978.5	
	Wet deposition	1688.9	
	Burden	11.89	11.84[c], 7.58−10.37[a]
	Lifetime	0.93	0.55−0.76[d]

Notes: References denote a, Liu et al. (2005); b for Textor et al., 2006, c derived from CMIP5 prescribed aerosol masses averaged from 1991 to 2000, d for Liu et al. (2012), and e for Liu et al. (2009); Ginoux et al. (2001)

https://doi.org/10.5194/gmd-2019-172
Preprint. Discussion started: 30 July 2019

Geoscientific Model Development Discussions
Open Access
EGU

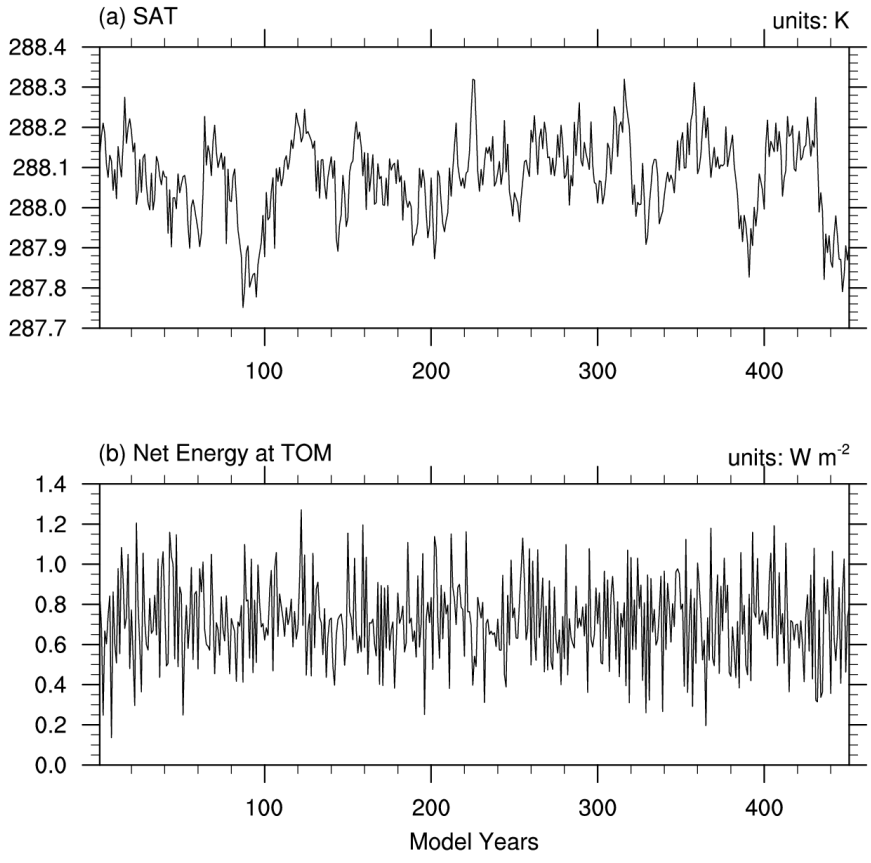

Figure 1. The time series of global and annual mean of (a) surface air temperature (K) and (b) net energy budget at top of the model (W • m^{-2}) in the last 450 years of a piControl simulation.

https://doi.org/10.5194/gmd-2019-172
Preprint. Discussion started: 30 July 2019

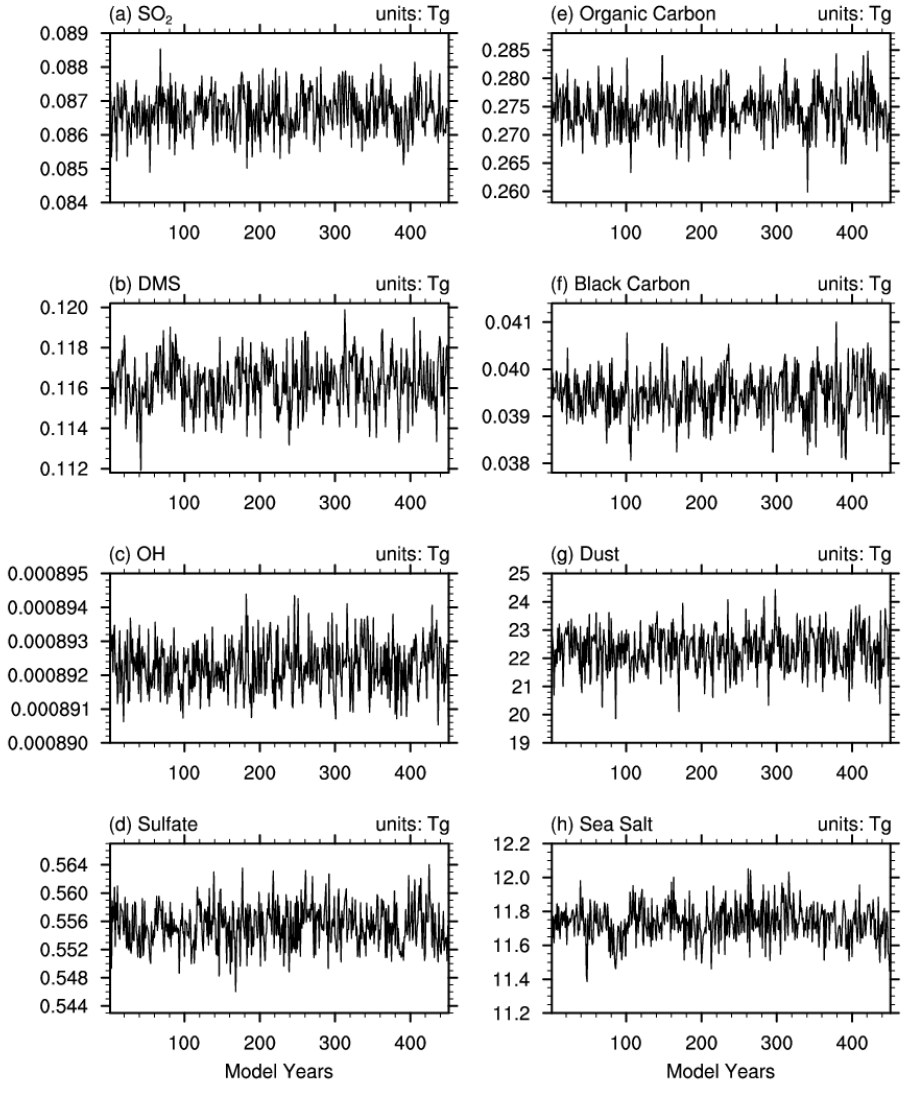

Figure 2. Same as in Figure 1, but for (a) SO_2, (b) DMS, (c) OH, and (d-h) different aerosols (in unit of Tg) in the troposphere (below 100 hPa).

https://doi.org/10.5194/gmd-2019-172
Preprint. Discussion started: 30 July 2019

Geoscientific Model Development Discussions

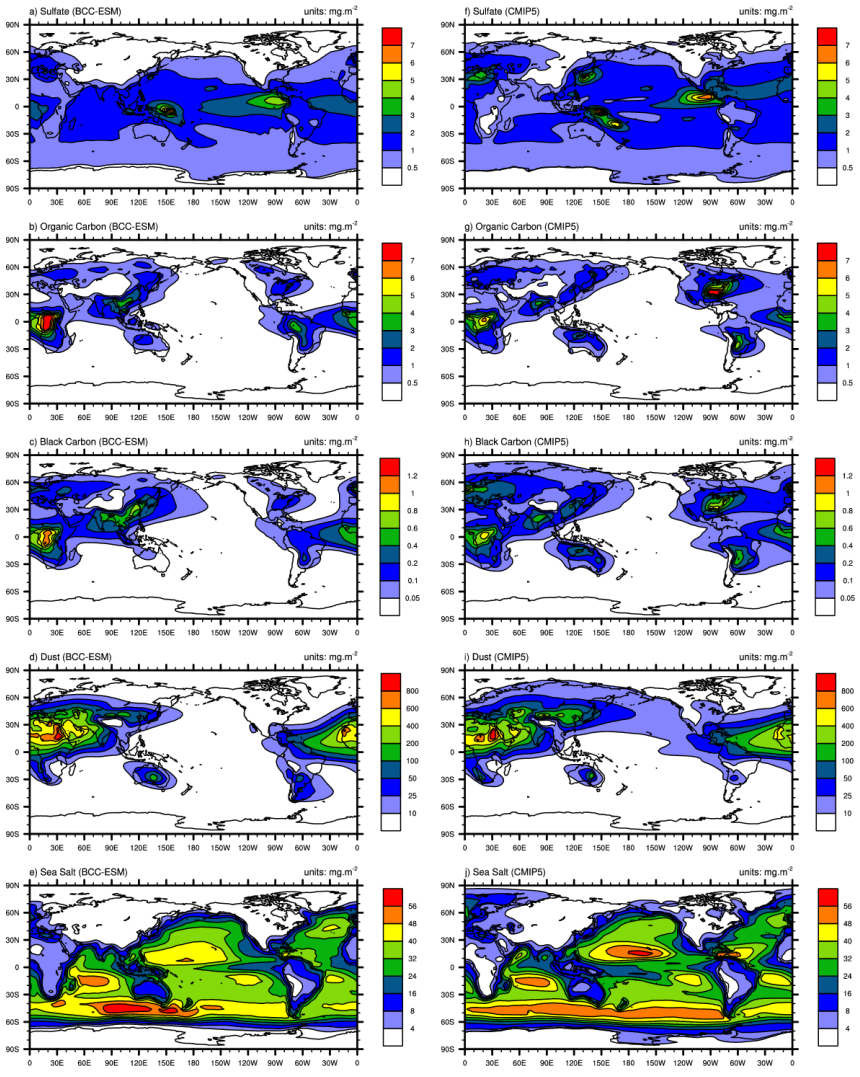

Figure 3. Global distributions of annual mean mass concentrations of sulfate (SO_4^{2-}; first row), organic carbon (OC; second row), black carbon (BC; third row), dust (fourth row), and sea salt (fifth row) aerosols in the whole atmospheric column. The left panels show the mean averaged for the last 100 years of BCC-ESM pre-industrial piControl simulations, and the right panels show the CMIP5 recommended aerosol concentrations in year 1850 (the website at IIASA http://tntcat.iiasa.ac.at/RcpDb/.). Units: mg m^{-2}.

https://doi.org/10.5194/gmd-2019-172
Preprint. Discussion started: 30 July 2019

Geoscientific Model Development Discussions
Open Access
EGU

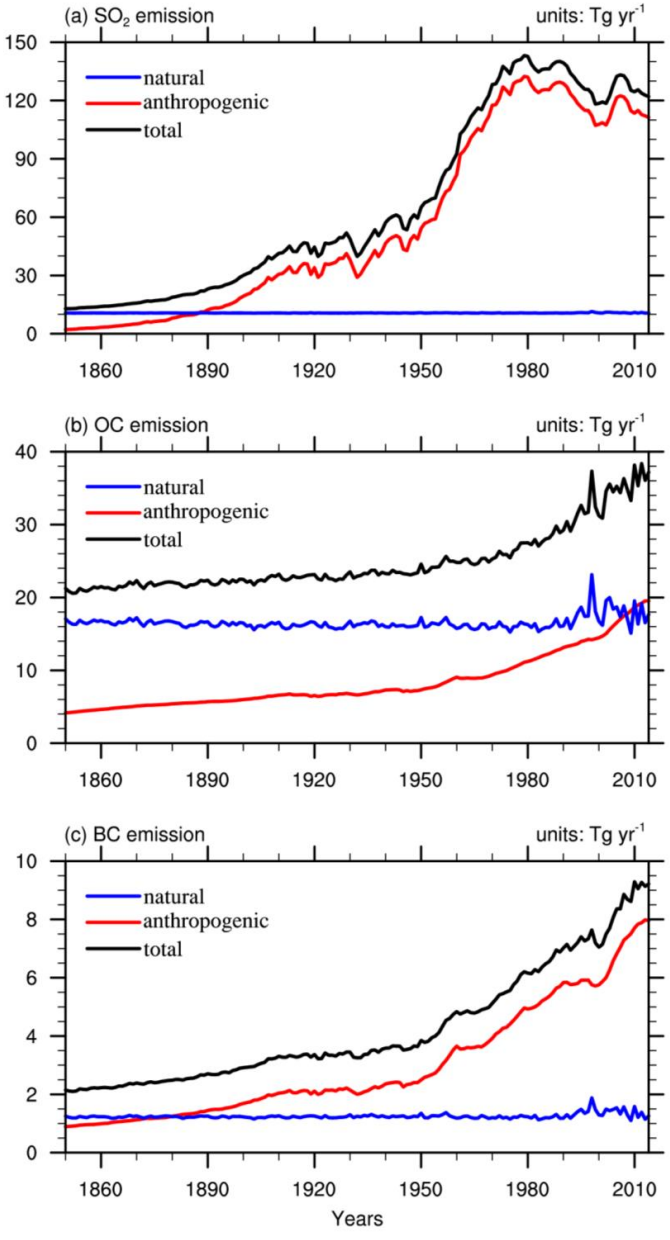

Figure 4. Global annual anthropogenic, natural, and total emissions of SO_2, organic carbon (OC), and black carbon (BC) in the BCC-ESM1 historical simulation. The units are Tg yr^{-1}.

https://doi.org/10.5194/gmd-2019-172
Preprint. Discussion started: 30 July 2019

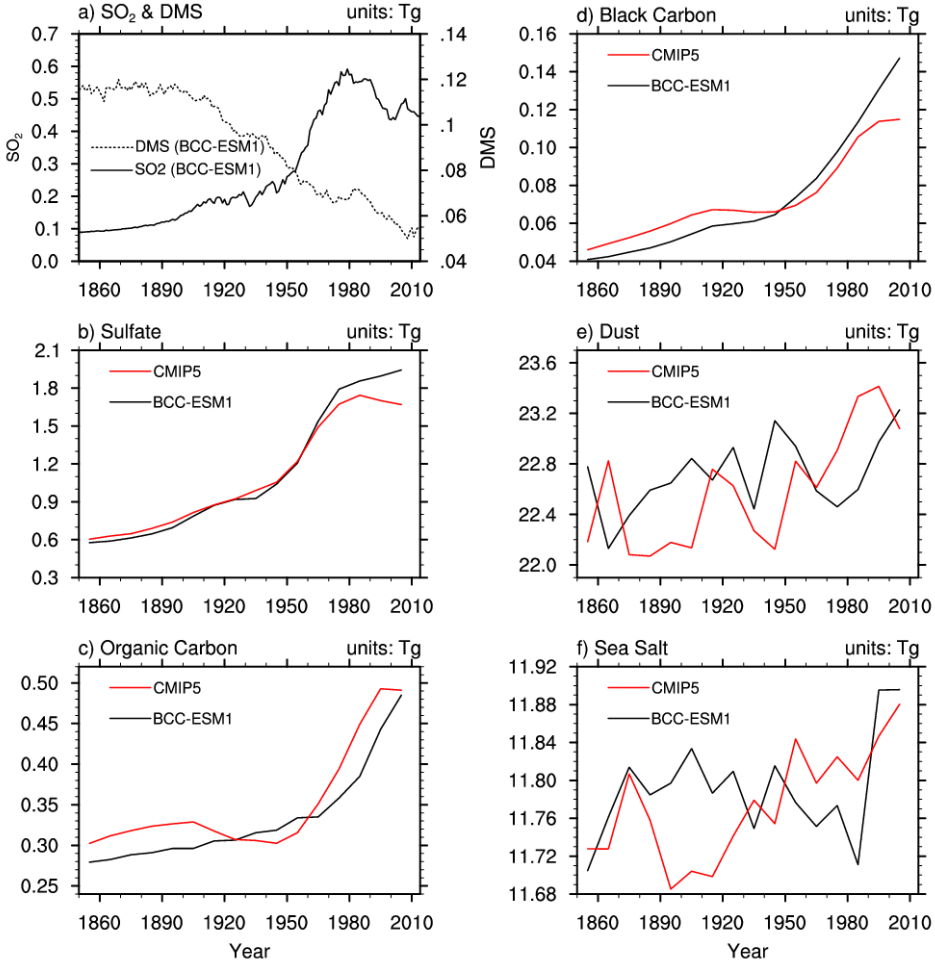

Figure 5. The time series of global annual amounts of (a) SO_2 and DMS and (b-f) aerosols in the whole atmosphere column from the 20th historical simulations of BCC-ESM1 (blue lines) and the CMIP5-recommended aerosols masses (red lines).

https://doi.org/10.5194/gmd-2019-172
Preprint. Discussion started: 30 July 2019

Geoscientific Model Development
Discussions
Open Access
EGU

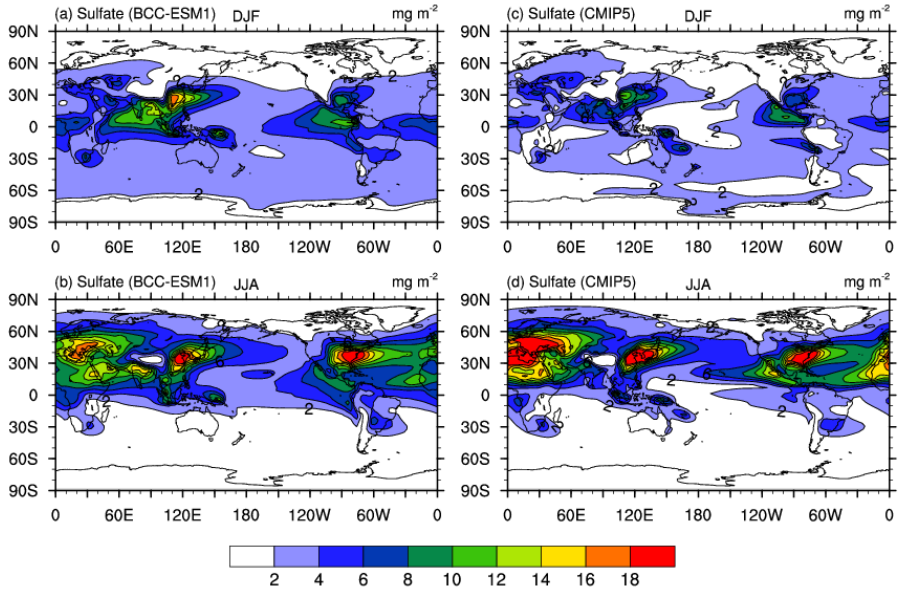

Figure 6. December-January-February (DJF; top panels) and June-July-August (JJA; bottom panels) mean sulfate (SO_4^{2-}) aerosol column mass concentrations averaged for the period of 1991-2000. Left panels show the historical simulations of BCC-ESM1, and right panels the CMIP5-recommended data. Units: $mg.m^{-2}$.

https://doi.org/10.5194/gmd-2019-172
Preprint. Discussion started: 30 July 2019

Geoscientific Model Development
Discussions
Open Access
EGU

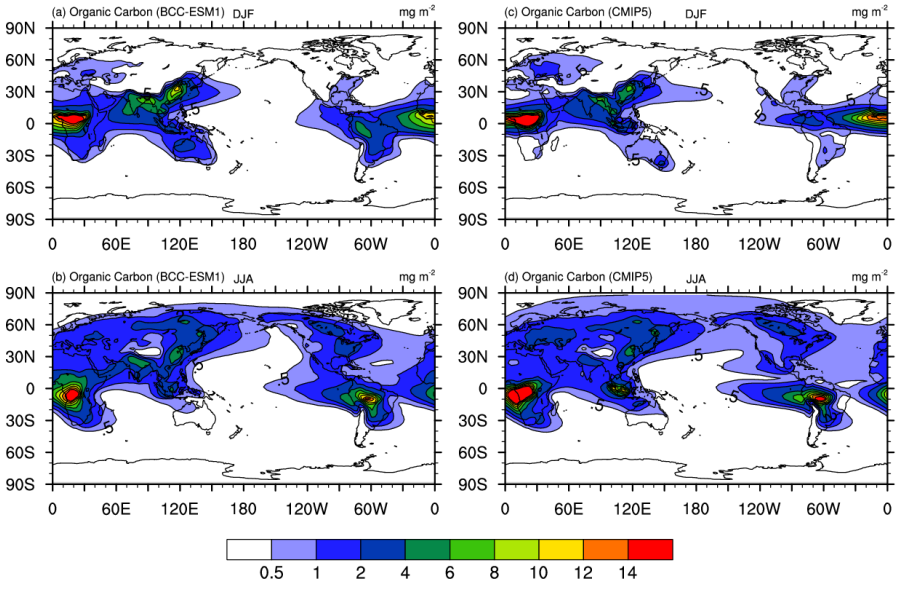

Figure 7. The same as in Figure 6, but for organic carbon (OC) aerosol column mass concentrations. Units: mg m^{-2}.

https://doi.org/10.5194/gmd-2019-172
Preprint. Discussion started: 30 July 2019

Geoscientific Model Development
Discussions
Open Access
EGU

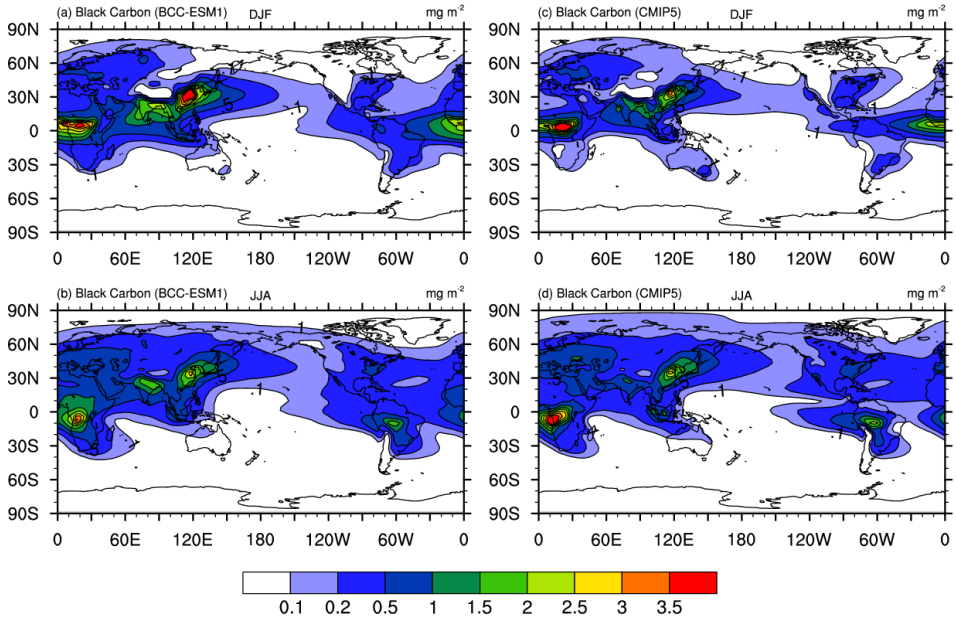

Figure 8. The same as in Figure 6, but for black carbon (BC) aerosol. Units: $mg.m^{-2}$.

https://doi.org/10.5194/gmd-2019-172
Preprint. Discussion started: 30 July 2019

Geoscientific Model Development Discussions
Open Access
EGU

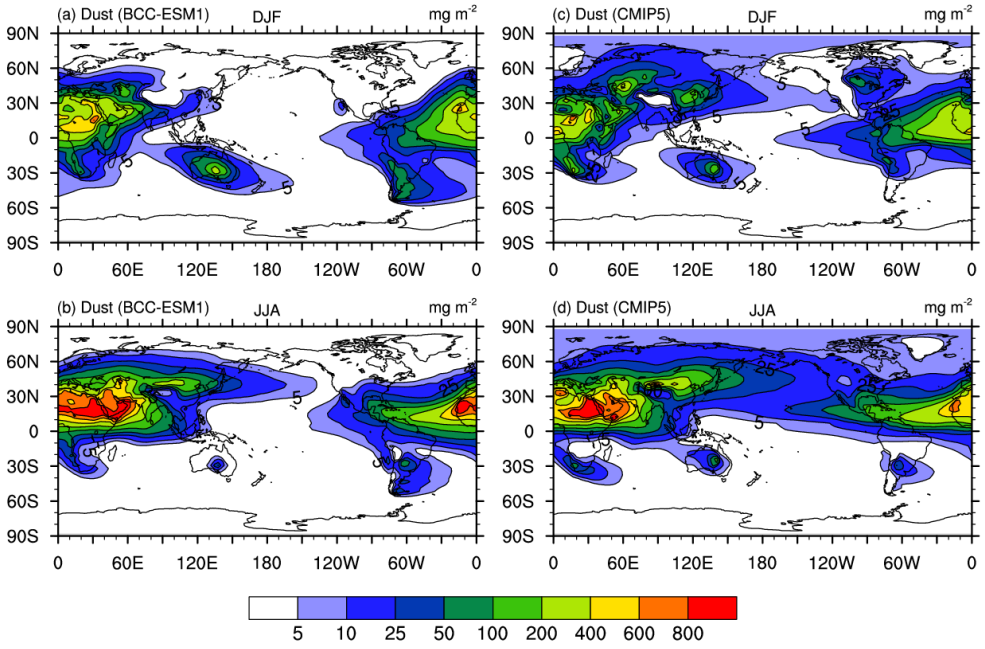

Figure 9. The same as in Figure 6, but for dust aerosol. Units: mg.m^{-2}.

https://doi.org/10.5194/gmd-2019-172
Preprint. Discussion started: 30 July 2019

Geoscientific Model Development Discussions
Open Access
EGU

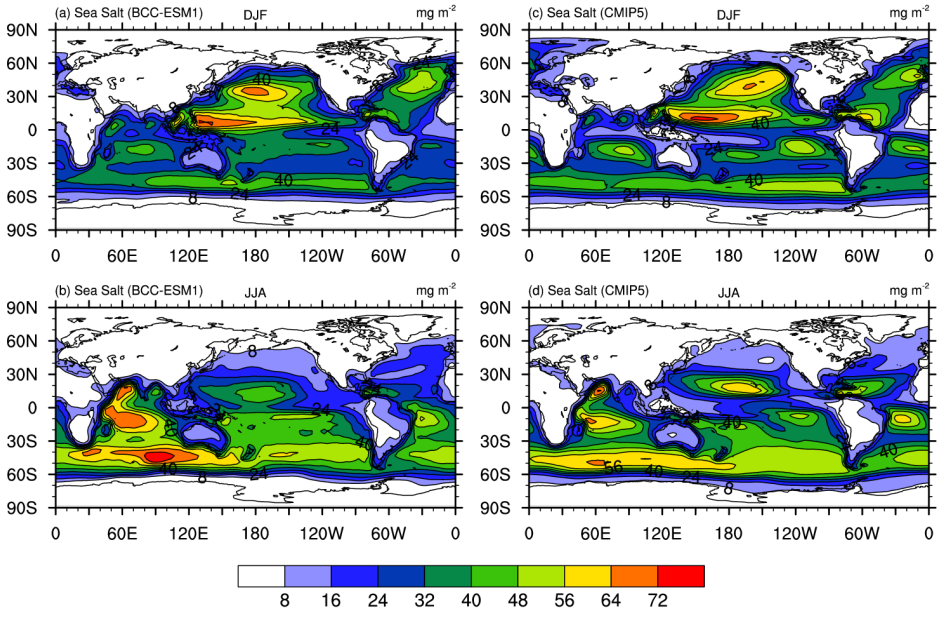

Figure 10. The same as in Figure 6, but for sea salt (SSLT) aerosol. Units: $mg.m^{-2}$.

https://doi.org/10.5194/gmd-2019-172
Preprint. Discussion started: 30 July 2019

Geoscientific Model Development Discussions

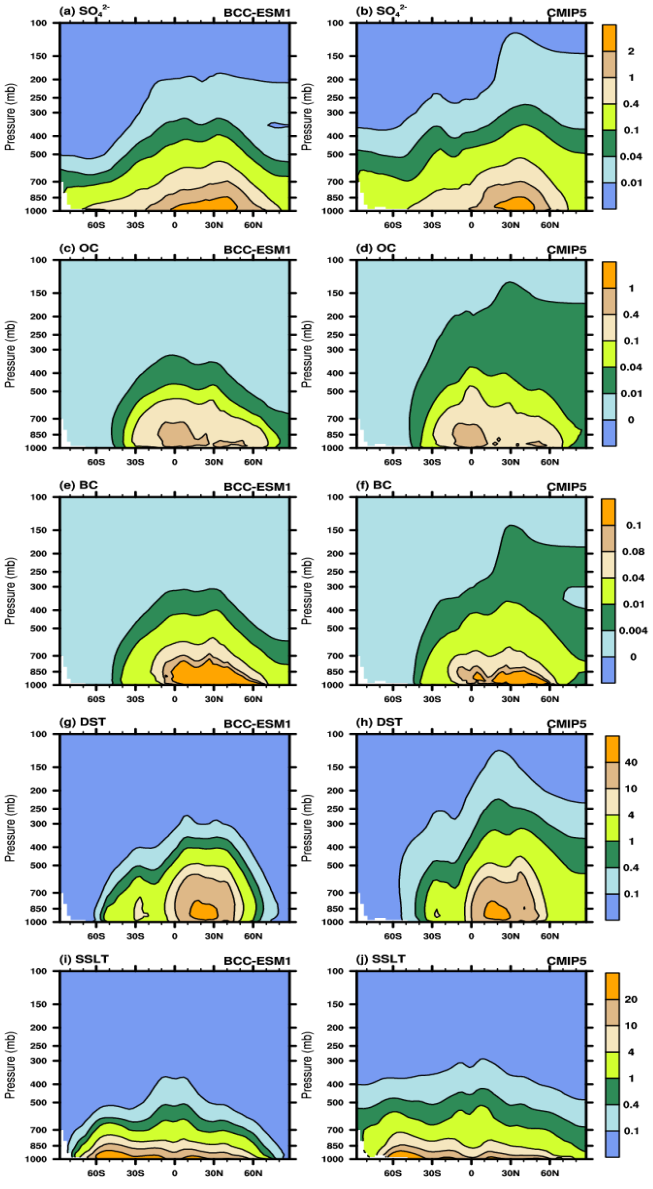

Figure 11. Latitude-pressure distributions of zonally-averaged annual mean sulfate, organic carbon, black carbon, dust, and sea salt aerosol concentrations for the period of 1991-2000. Left panels show the 20th century historical simulation of BCC-ESM1, and right panels the CMIP5 recommendation data. Units: μg m^{-3}.

https://doi.org/10.5194/gmd-2019-172
Preprint. Discussion started: 30 July 2019

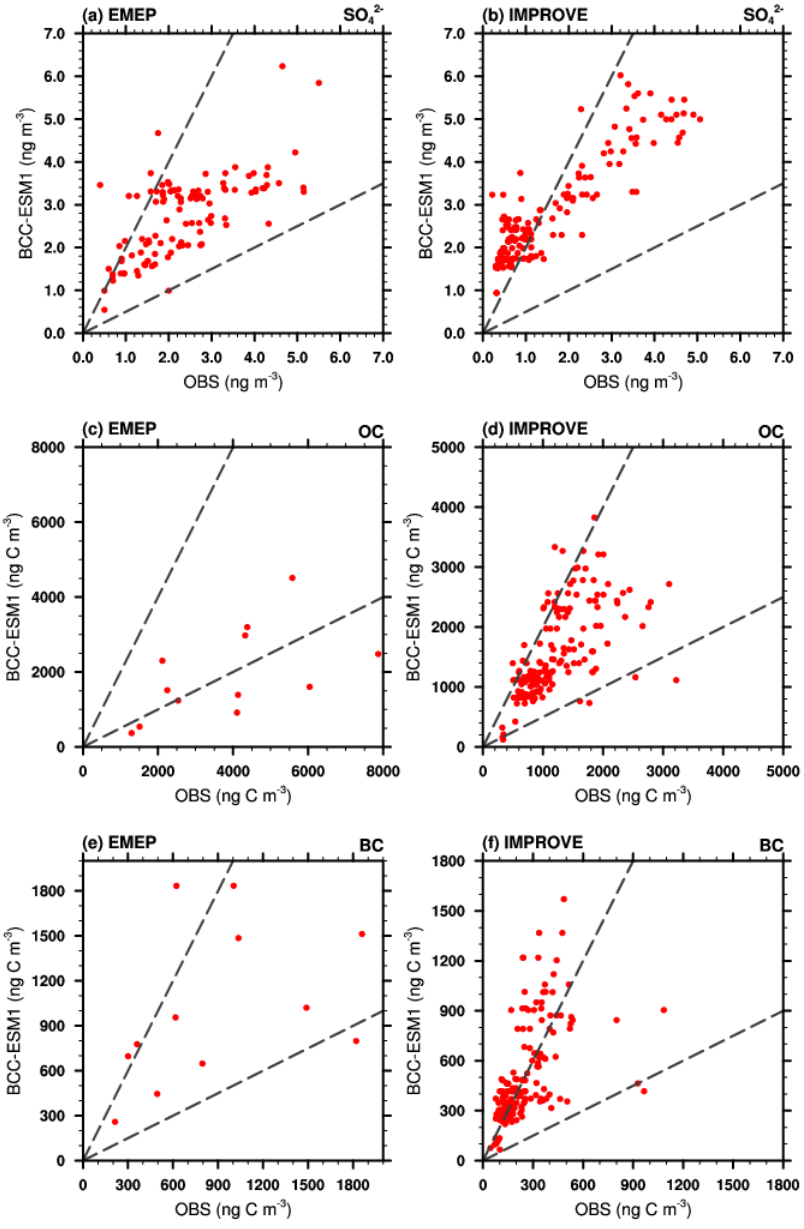

Figure 12. Scatter plots showing observed versus simulated annual mean sulfate (SO_4^{2-}), organic carbon (OC), black carbon (BC) mixing ratios at IMPROVE and EMEP network sites. Observations are averages over the available years 1990–2005 for IMPROVE sites, and 1995–2005 for EMEP sites. Simulated values are those at the lowest layer of BCC-ESM1.

https://doi.org/10.5194/gmd-2019-172
Preprint. Discussion started: 30 July 2019

Geoscientific Model Development Discussions
Open Access
EGU

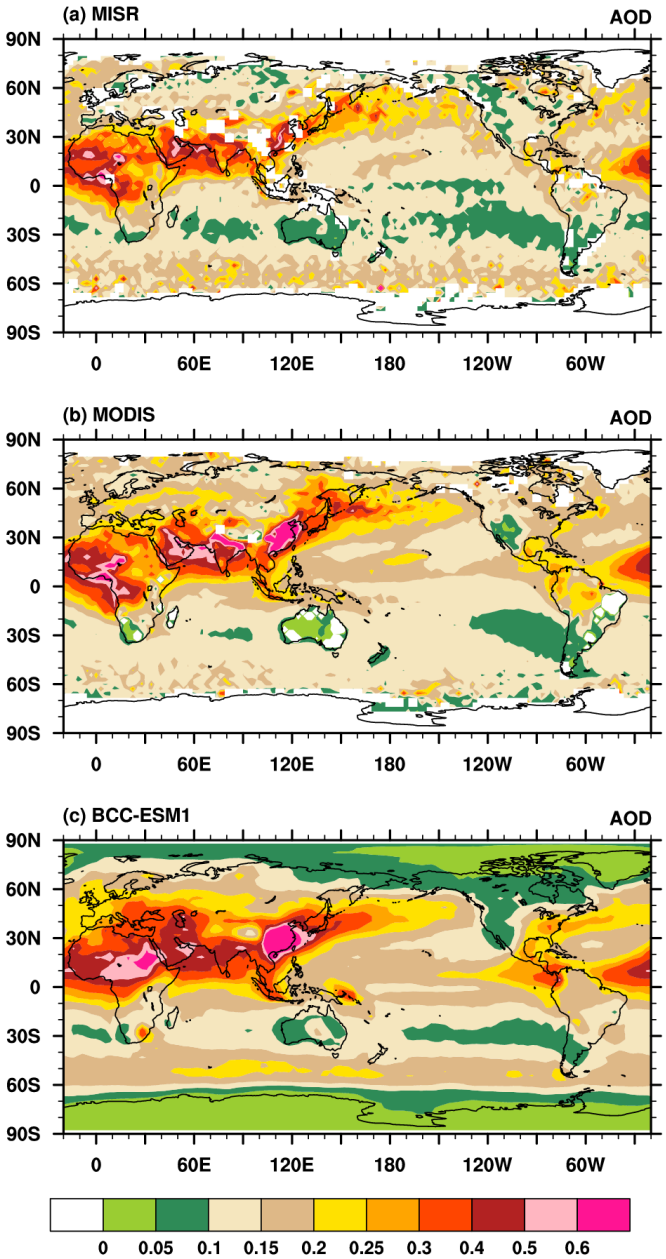

Figure 13. Global distribution of annual mean AOD simulated in BCC-ESM1 compared with the MISR and MODIS data for the year 2008.

https://doi.org/10.5194/gmd-2019-172
Preprint. Discussion started: 30 July 2019

Geoscientific Model Development Discussions

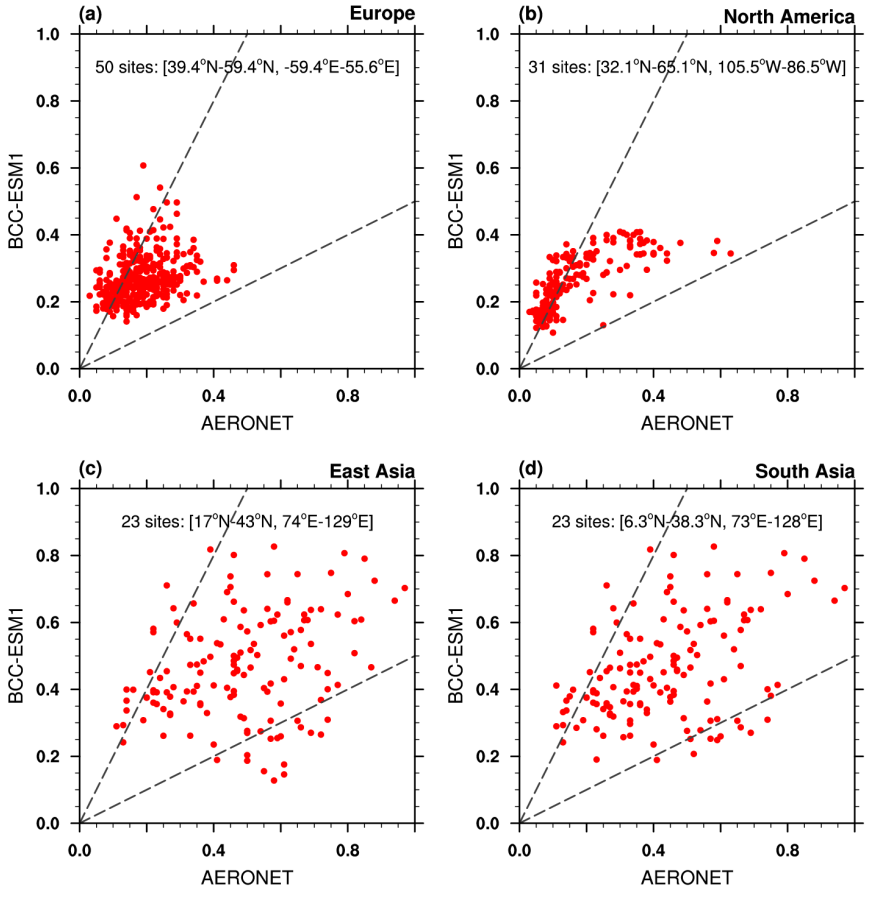

Figure 14. Scatter plots of observed versus simulated monthly mean AOD at AERONET sites in Europe, North America, East Asia, and South Asia. Each data point represents an available monthly mean AOD at a site and its corresponding model result over 1998-2005.